HEALTH ASSESSMENTS OF RIPARIAN FORESTS USING THE LANDSAT ARCHIVE

OSCAR ROBERT ZIMMERMAN
Bachelor of Science, University of British Columbia, 2019

A thesis submitted
in partial fulfilment of the requirements for the degree of

MASTER OF SCIENCE

in

ENVIRONMENTAL SCIENCE

Environmental Science Program
University of Lethbridge
LETHBRIDGE, ALBERTA, CANADA

HEALTH ASSESSMENTS OF RIPARIAN FORESTS USING THE LANDSAT ARCHIVE

OSCAR ROBERT ZIMMERMAN

Date of Defence: August 18, 2021

Dr. L. B. Flanagan Thesis Supervisor	Professor	Ph.D.
Dr. S. B. Rood Thesis Examination Committee Member	Professor Emeritus	Ph.D.
Dr. C. A. Coburn Thesis Examination Committee Member	Professor	Ph.D.
Dr. R. M. Golsteyn Chair, Thesis Examination Committee	Associate Professor	Ph.D

Abstract

The archive of satellite imagery from the Landsat Program between 1984 and 2020 was leveraged to assess the health status of riparian cottonwood forests along the regulated Oldman River in semi-arid southern Alberta, Canada. An extension of the near-infrared reflectance of vegetation, NIRvP, was adopted as a health indicator and validated to be a practical yet meaningful proxy of primary production. NIRvP was correlated with streamflow and a climatic soil moisture index from year-to-year. Forests responded to reduced streamflow with curtailed productivity, but were vigorous with return of adequate moisture. Forests did not respond to low flow characteristics, including reoccurring dewatering during the mid–late summer in years prior to the Oldman River Dam. These results supported that cottonwoods avoided, resisted, and were resilient to relatively short drought-like conditions imposed by streamflow reductions. Under current conditions, the outlook on the health of the riparian corridor is positive.

Acknowledgments

I thank Dr. Larry Flanagan for warmly welcoming me to the University of Lethbridge, his mentorship, and encouragement. I thank Dr. Stewart Rood for his mentorship, enthusiasm, and providing me with opportunities beyond the scope of my thesis work. I thank Dr. Craig Coburn for his involvement in my thesis supervisory committee. I am thankful for financial support received in the form of graduate assistantships and awards from the University of Lethbridge.

Contents

List of Tables

List of Figures

List of Symbols and Abbreviations

BAI	Basal area increments
ETM+	Enhanced Thematic Mapper Plus
GPP	Gross primary production
HSNR	Helen Schuler Nature Reserve
LNID	Lethbridge Northern Irrigation District
MODIS	Moderate Resolution Imaging Spectroradiometer
NDVI	Normalized difference vegetation index
NIRv	Near-infrared reflectance of vegetation
NIRvP	Near-infrared reflectance of vegetation multiplied by a radiation constraint
NEE	Net ecosystem carbon dioxide exchange
OLI	Operational Land Imager
ρ_s	Spearman's rank correlation coefficient
r^2	Coefficient of determination
RI	Radial increments
RMSE	Root mean squared error
SMI	Soil moisture index
TM	Thematic Mapper
WRS-2	World Reference System-2

Chapter 1

Introduction

1.1 Background

Across the western North American prairies, rivers draining the continent's water towers in the Rocky Mountains provide new opportunities for life within the semi-arid landscape. Rivers provide the freshwater source for large-scale food production through irrigated agriculture, and the people and industries that this prospect brings. Interfaces between rivers and the adjacent terrestrial environment also contribute greatly to the diversity of species and ecological functions at the landscape-scale (Naiman et al., 1993; Naiman & Decamps, 1997). River floodplains contain patchworks of resource rich habitats that allow for the survival of relatively mesic species, boasting woodlands and gallery forests to a landscape dominated by grasses and short stature shrubs (Bradley et al., 1991; Naiman et al., 1993; Patten, 1998).

Cottonwoods (riparian *Populus* species) are the foundation species of riparian forests in the semi-arid prairies, and often the exclusive trees (Bradley et al., 1991; Ellison et al., 2005; Patten, 1998). River floodplains offer the ideal habitat for cottonwoods (Figure 1.1); pulses of geomorphic disturbance associated with periodic floods generate moist and barren seedbeds for establishment of shade intolerant seedlings (Braatne et al., 1996). Streamflow also sustains relatively shallow alluvial groundwater tables, which supplement the sparse precipitation and provide the essential moisture subsidy for tree survival in the semi-arid climate (Rood et al., 2003; Tai et al., 2018; Yang et al., 2019). Cottonwoods are adapted to thrive in the dry climate

Figure 1.1: Cottonwoods are restricted to river floodplains in the western North American prairies, as depicted here at the confluence of the Oldman and St. Mary Rivers in southern Alberta, Canada.

and the seasonally dynamic moisture environment typical along nival rivers (Kranjcec et al., 1998; Rood et al., 2000, 2011).

The functions of riparian forests as hotspots of biodiversity, nutrient filters, barriers to bank erosion, and recreation areas represent non-monetized naturally occurring services that are beneficial for humans (Bradley et al., 1991; Naiman & Decamps, 1997; Patten, 1998), yet human alterations of rivers threaten the survival of these ecosystems which depend on instream flows and the river's natural hydrological and geomorphic dynamism (Braatne et al., 1996; Lytle & Poff, 2004; Stromberg, 2001). Human activities that involve chronic water removal from the river channel, such as offstream diversion, subject cottonwoods to stressful conditions that are analogous to prolonged drought (Rood et al., 2003). Growth declines, partial dieback, and complete collapses of riparian forests have been documented downstream of diversion structures across semi-arid and arid North America (Nagler et al., 2020; Rood et al., 1995; Schook et al., 2020; Smith et al., 1991; Williams & Cooper, 2005). While completely

restoring naturally occurring flow regimes is not practical, there is an urgency to provide functional flow regimes on regulated rivers that support the conservation of downstream ecosystems (Rood et al., 2005; Stromberg, 2001).

The Oldman River Basin in southern Alberta, Canada is heavily allocated, primarily for agricultural irrigation (Benson & Rood, 2018). Since its completion in 1993, the Oldman River Dam has operated to deliver functional flows for downstream ecosystems, particularly cottonwood forests (Rood et al., 2005). Dam operations have supported both irrigation expansion and the naturalization of instream flow conditions during the mid–late summer months that were progressively degraded throughout the twentieth century (Rood et al., 2005). Climate change, population growth, and increasing economic activity pose ongoing pressures on water resources in the Oldman River Basin (Schindler & Donahue, 2006; St. Jacques et al., 2010, 2013). An optimization of current dam operations would be desirable to maximize allocatable water in the future (Benson & Rood, 2018). As a first step, the current health status of riparian forests along the Oldman River must be reviewed. Bradley et al. (1991) assessed historical changes in forest cover using airphotos, however similar historical health assessments of mature groves have not been revisited since the Oldman River Dam Project. This raises the fundamental questions, what is the current health of riparian forests along the Oldman River? How have dam operations contributed to their health? Here, the ecosystem's health is synonymous with its ability to obtain resources for primary production, the fundamental metabolic process that supports its broader ecological function and capacity to provision valued services. Inherently, its health is related to the health of cottonwoods; while younger individuals that rejuvenate aging populations are invaluable, mature individuals are of greater significance to this working definition of health—at least at relatively short timescales. The benefits of functional flows for seedling establishment along the Oldman River have been documented by previous workers (Rood et al., 1998, 2005).

Satellite remote sensing has been widely adopted as a tool for ecological monitoring of riparian forests along allocated rivers, with studies in arid regions of the United States, Mexico, China, and Australia sharing the common goal of providing ecosystem health indicators to inform riparian conservation (Doody et al., 2014; Gómez-Sapiens et al., 2020; Nagler et al., 2009, 2020; Zhao et al., 2016). Satellite remote sensing expands the spatial scope of traditional vegetation monitoring by providing a means of scaling calibrated health indicators across entire river corridors, allowing for wide-area sampling and spatially distributed health assessments (Nagler et al., 2009). Additionally, long-running Earth observation programs such as Landsat offer historical insight into patterns of health at timescales of years–decades (Huntington et al., 2016; Nguyen et al., 2015; Zhao et al., 2016). Most previous workers have adopted spectral vegetation indices as health indicators, which are fundamentally related to the structure of the plant canopy and its capacity for visible light absorption and primary production (Field, 1991; Sellers, 1987).

This thesis leveraged satellite remote sensing, specifically the archive of imagery provided by the Landsat Program, to make historical health assessments of riparian forests along the Oldman River at spatial scales of single groves to the entire river corridor. The first interest of this thesis was related to the development of an ecologically meaningful satellite imaging tool. During the past several years, the near-infrared reflectance of vegetation (NIRv) has emerged as a practical approach to inferring terrestrial primary production, based on the same fundamental principles as vegetation indices (Badgley et al., 2017, 2019). The ability of NIRv to reduce the confounding contribution of soil to land surface reflectance, its interpretation as an estimated biophysical parameter, and its empirical links to far-red sun-induced chlorophyll fluorescence suggests an advancement from traditional vegetation indices as a proxy for primary production (Badgley et al., 2017; Dechant et al., 2020; Zeng et al., 2019). Records of ecosystem gas exchange and annual cottonwood growth that

were available along the Oldman River made it possible to validate NIRv at various temporal and biological scales. Once this tool was developed, the primary interest was assessment of temporal variation. With the temporal domain of the Landsat archive, it was possible to assess health in time periods both prior-to and after the Oldman River Dam Project. A second interest was related to spatial variation, particularly the effect of dam operations on health along different reaches—river segments with distinct hydrology, geomorphology, or human impacts—of the Oldman River. There was also a question related to differences in how cottonwoods function along a transition from foothills to prairie ecoregions (Kranjcec et al., 1998; Rood et al., 2011; Tyree et al., 1994).

1.2 Research objectives, hypotheses and thesis layout

The objectives of this thesis were the following:

1. Validate NIRv as a proxy for primary production and ecosystem health indicator in a riparian cottonwood forest ecosystem.

2. Assess temporal patterns of riparian forest productivity relative to climate and streamflow conditions using NIRv derived from historical Landsat images.

3. Assess spatial patterns of productivity among three reaches of the Oldman River with different levels of streamflow regulation.

Several hypotheses were made with regards to the anticipated year-to-year patterns of productivity. First, interannual variability in productivity was anticipated to be associated with growing season streamflow along all reaches. Second, productivity was anticipated to increase in post-dam years along heavily allocated reaches, due to naturalization of streamflow conditions during the mid–late summer months; along less allocated reaches, no-long term trend was anticipated. Lastly, the correlation between streamflow and productivity was anticipated to be stronger at increasingly

arid lower elevation reaches, due to greater moisture limitation. The remainder of the thesis is organized as follows: a description of the study area, datasets, and the analysis are provided in Chapter 2; results are presented in Chapter 3; results are discussed and conclusions are made in Chapter 4; supplementary methods and results are provided in two appendices.

Chapter 2

Methods

2.1 Study area description

2.1.1 Introduction and location

The Oldman River Basin nests in the southwestern corner of Alberta, Canada, where the prairies meet the eastern hillslopes of the Rocky Mountains (Figure 2.1). Its mainstem, the Oldman River, flows 363 km to the east before joining the Bow River to form the South Saskatchewan River. Two thirds of flows on the Oldman River and more than three quarters of flows on its southern tributaries are allocated offstream, primarily for agricultural irrigation (Benson & Rood, 2018). Approximately 70% of the natural land cover within the basin has been converted from native prairie, mostly for agriculture and some ranching in the foothills and prairie regions (Oldman Waterhsed Council, 2010). Prior to European contact, Blackfoot speaking people including the *Káínaa* and *Piikáni* hunted buffalo in the basin. The Oldman River lies at the center of their homeland, which, according to their tradition, was set forth by The Creator *N'api*—"Old Man". The focus of this study were the reaches downstream of the Oldman River Dam, where transitional upland groves of aspen and pine that scatter the foothills disappear from the prairie landscape, revealing riparian cottonwoods as the exclusive trees.

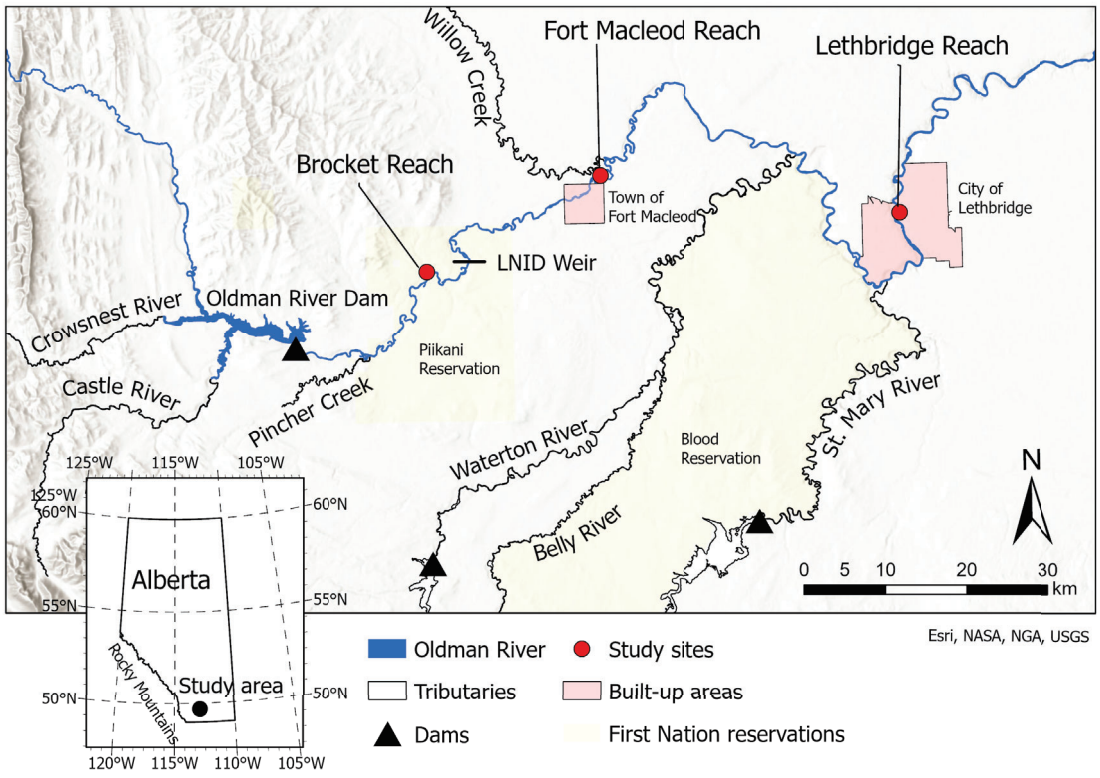

Figure 2.1: Map of the study area in southern Alberta, Canada.

2.1.2 Climate, hydrology and geomorphology

The climate is typical of the semi-arid prairies, with cold winters and warm summers. Although winters are on average subzero, snowpacks are short-lived due to frequent Chinook winds and associated warming. Mean annual precipitation is around 400 mm, with approximately two thirds falling as rain within the core growing season months of May–September. Precipitation is greatest in June, followed by May, and tapers throughout the rest of the year. The mid–late summer is warm and dry. With the exception of its upper-catchments, the basin experiences a climatic moisture deficit (annual potential evapotranspiration exceeds precipitation) that generally increases with distance from the foothills.

Snowmelt in the basin's Rocky Mountain headwaters is the primary mechanism of streamflow generation. The seasonal hydrograph is typical of nival rivers; flows rise in the spring to a peak in June, rapidly recede in July, then gradually recede to

baseflow conditions throughout the remainder of the summer and autumn. Spring and summer rainstorms are smaller contributors to streamflow generation, though intense rainfall on upper-catchment soils moistened by snowmelt trigger high flows, including floods (Rood et al., 1998). Several large-scale climate patterns that influence winter alpine precipitation are linked with interannual streamflow variability, most notably the Pacific Decadal Oscillation (Rood et al., 2013; St. Jacques et al., 2010).

Rivers occur in coulee systems which consist of a main valley, formed by postglacial stream networks, and short and straight dry tributary valleys. The width of the main valley lays a constraint on river meandering, with its longitudinal variation resulting in the occurrence of both unconstrained broad alluvial valleys and constrained straight narrow canyons along the river corridor. Highly permeable mixtures of sand, gravel, and cobble form the typical substrate of the river floodplain (Rood et al., 1995, 2013). For most of the year the alluvial groundwater table slopes away from the river, rising and falling in concert with the river water surface with only slight lags in infiltration and drainage (Rood et al., 2013). Infiltrating river water is the primary mode of alluvial groundwater recharge (Flanagan et al., 2019).

2.1.3 Vegetation

Three species of cottonwood occur at the boundaries of their geographic distributions and naturally hybridize within the floodplain of the Oldman River (Bradley et al., 1991). Their distribution reflects gradients of moisture within the basin; prairie cottonwoods (*Populus deltoides*) occur at the western limit of their range, balsam poplars (*P. balsamifera*) occur at their southeastern limit, and the intermediate narrowleaf cottonwoods (*P. angustifolia*) occur at their northeastern limit. The understory of cottonwood forests consists of a herbaceous community and a variety of shrubs, including buffaloberry (*Shepherdia argenta*), wolf willow (*Elaeagnus commutata*), and chokecherry (*Prunus virginiana*). Cottonwoods flush new leaves in early May and the

canopy is at full maturity by the end of June. The timing of leaf flush is more-less consistent along the river, due to photoperiodic controls to avoid frost damage of catkins, as is autumnal leaf senescence and abscission in early–mid October. Drought deciduousness is not displayed, but precocious senescence of individual branches or patches of foliage in July and August is a common drought response of cottonwoods that is related to xylem cavitation (Rood et al., 2000). Contrary to the seasonal phenology of cottonwoods, the phenology of regional prairie grassland communities are driven by booms and busts in rainfall, reflecting their differential access to sources of moisture (Flanagan & Adkinson, 2011; Yang et al., 2019).

2.1.4 River regulation and management

Offstream diversion of the Oldman River began in the 1920's to supply the Lethbridge Northern Irrigation District (LNID) through a network of canals and small offstream reservoirs (Rood & Vandersteen, 2010). The primary diversion structure, the LNID Weir, remains operational today (Figure 2.1). Despite major dam projects on its southern tributaries—the St. Mary Dam was completed in 1951, and the Waterton Dam in 1964—the Oldman River lacked an onstream storage structure until the Oldman River Dam Project (1988–1992). As a result, low flows progressively declined throughout the twentieth century, reflecting increasing water diversion during the summer months to meet growing irrigation demands (Figure 2.2). During the 1980's, streamflow was as low as 5% the natural condition during the dry mid–late summer (Rood & Vandersteen, 2010), and this was presumably unfavourable for cottonwoods.

The Oldman River Dam traps abundant spring flows for gradual release during the summer months when irrigation demands peak. In response to environmental concerns, allocation of stored water was prioritized to meet minimum flow requirements that were revised in 1993 for ecosystem instream flow needs (Rood & Vandersteen, 2010). Consequently, dam operations enabled a more naturalized streamflow con-

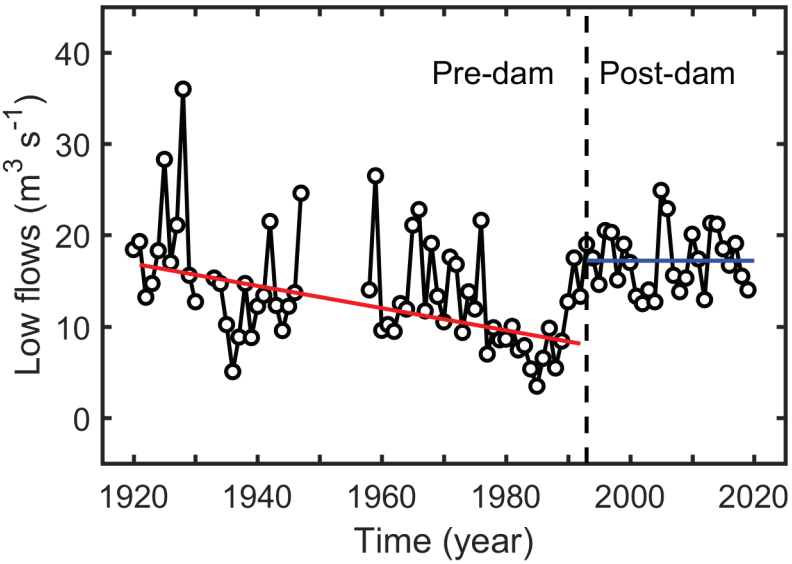

Figure 2.2: Low flows (annual tenth percentile flow) for the Oldman River through the City of Lethbridge. The dashed vertical line marks the inception of the Oldman River Dam in 1993.

dition during the mid–late summer (Figure 2.2). The dam also operates to deliver "ramped flows", a manipulated gradual recession of the hydrograph in flood years to facilitate cottonwood seedling establishment (Rood et al., 1998). The Oldman River Dam Project led to the immediate adoption of these operations by both the St. Mary and Waterton Dams. Thus, dams across the Oldman River Basin currently operate to collectively deliver functional flow regimes that are beneficial for downstream cottonwoods (Foster et al., 2018; Rood & Mahoney, 2000; Rood et al., 2005). With current dam operations, the seasonal hydrograph is on average naturalized. However, storage dampens its seasonal flashiness and in drought years there can be partial–near complete attenuation of the hydrograph's crest.

2.1.5 Study sites and reaches

The primary study site was a mixed prairie and narrowleaf cottonwood forest located within the Helen Schuler Nature Reserve (HSNR) in the Oldman River valley through the City of Lethbridge (Figure 2.1). The HSNR is a site of ongoing research on riparian

cottonwoods and has been described in detail elsewhere (Flanagan et al., 2017; Rood et al., 2013). The site was studied as representative of the entire Lethbridge Reach, which begins at the St. Mary River inflow and extends through the City of Lethbridge, to remain consistent with remote sensing validation exercises that were undertaken (Section 2.6). Flows are impacted by diversions and reservoirs on the Oldman River and its southern tributaries.

To extend the spatial scope of the study, cottonwood forests were also studied along two other reaches of the Oldman River. The Fort Macleod Reach extended for 12 km, beginning in the Town of Fort Macleod and terminating several kilometers downstream of the Willow Creek inflow (Figure 2.1). Forests within the generally wide alluvial valley floodplain contained primarily narrowleaf cottonwoods, as well as balsam poplars (Willms et al., 2006). The Fort Macleod Reach is upstream of the southern tributaries but is still impacted by the diversion at the LNID, reflecting an intermediate reach. The Brocket Reach extended for 6 km within the Piikani Reservation upstream of the LNID Weir (Figure 2.1), and was within the natural range of balsam poplars and narrowleaf cottonwoods. Prior to the Oldman River Dam, the Brocket Reach was free-flowing. Current dam operations have a slight–moderate impact on streamflow, primarily altering its seasonal timing. The Brocket Reach was the least regulated study reach, acting as a standard reference.

The areas for remote sensing analysis, described next, were manually digitized with aid from a high resolution basemap and chosen to contain mature cottonwood canopy as the primary land cover.

2.2 Satellite imagery

Images from the Landsat 5 Thematic Mapper (TM), Landsat 7 Enhanced Thematic Mapper Plus (ETM+), and Landsat 8 Operational Land Imager (OLI) were combined, providing imagery from 1984 to 2020 at a 30 m spatial resolution for six com-

mon reflective wavebands. Collection 1 Level 1 data products were used, which are precision- and terrain-corrected to the highest standard and processed to surface reflectance using the Landsat Ecosystem Disturbance Adaptive Processing System for TM and ETM+, and the Landsat Surface Reflectance Code for OLI. Images from a central World Reference System-2 (WRS-2) Path/Row (41/25) and two overlapping WRS-2 Paths (42 and 40) were used. Only images with <75% cloud cover within the entire image or a subscene containing the study area were accepted. The pixel quality assessment band was used to mask clouds and cloud shadows, which were buffered by 300 m, and snow pixels were flagged and dealt with at a later stage. The global surface water dataset (Pekel et al., 2016) was used to mask the occurrence surface water since 1984, which was buffered by 30 m. Images were accessed from the Google Earth Engine (`https://earthengine.google.com/`) and exported out of the Google Cloud for further analysis in MATLAB (Version 9.0, The Mathworks, Natick, MA, USA).

Combining images from TM, ETM+, and OLI can result in biases in the reflectance time series due to differences in sensor design, sensor spectral response, or atmospheric correction (Holden & Woodcock, 2016; Roy, Kovalskyy, et al., 2016). To account for this, the method of Roy, Kovalskyy, et al. (2016) was adopted to normalize TM and OLI reflectance to ETM+-like values. In brief, images overlapping with one-day separation between adjacent WRS-2 Paths were used to generate linear equations that predicted ETM+-like reflectance on a band basis. Another bias has been noted in studies that combine images from adjacent WRS-2 Paths, related to view angle effects on reflectance at the overlapping image margins (Sulla-Menashe et al., 2016). A second set of linear correction equations were generated to account for this that normalized reflectance from WRS-2 Path 40 and 42 images to values as if viewed from Path 41. An extended methods, including an evaluation of the harmonized data product against the Moderate Resolution Imaging Spectroradiometer, is provided in Appendix A.

2.3 Remotely sensed proxy: NIRvP

The near-infrared reflectance of vegetation (NIRv) was calculated from Landsat images as the product of the near-infrared reflectance and normalized difference vegetation index (NDVI) (Badgley et al., 2017). By definition of NIRv, this product estimates the contribution of green vegetation to the total scene reflectance to near-infrared light (Badgley et al., 2017; Zeng et al., 2019). To account for spatial and temporal differences in non-zero NIRv during the dormant season, the NDVI during these months within a three year-minimum moving window was subtracted from NDVI before multiplication. Zeng et al. (2019) recommended using a scaled NDVI that also accounts for the underestimation of the actual near-infrared reflectance of vegetation at high leaf area index, but this method was not adopted due to ambiguity in defining a maximum NDVI—the NDVI as the fractional vegetation cover approaches one—from observation records. This was also likely to be a small issue given the relatively low leaf area index of the riparian corridor (estimated 1.4 m^2 m^{-2}, Flanagan et al. 2017). NIRv of pixels that were flagged as snow were set to zero at this time.

As an extension, NIRv was constrained by the seasonal course of downwelling solar radiation. Specifically, NIRv was multiplied by the top of atmosphere irradiance for the corresponding day (following Monteith & Unsworth 2013) divided by its annual maximum value for that location, hereby referred to as NIRvP. This naming was based on Dechant et al. (2020), though their NIRvP was calculated by multiplying NIRv by instantaneous fluxes of downwelling photosynthetically active radiation ("P") to estimate NIRv in radiance units (see also Baldocchi et al. 2020; Wu et al. 2020). Based on the results from a validation of NIRv against ground data on primary production (Section 2.6), the radiation constraint was adopted for the remainder of the study.

Pixel time series of NIRvP were fit with cubic smoothing splines (*csaps* function in MATLAB) to retrieve continuous daily values. To assure quality, two measures were

taken. First, a moving window method was used to detect dark spikes in NIRv (e.g. undetected cloud, cloud shadow, haze) before fitting cubic-splines. An observation was removed if it met the conditions $(\mathrm{NIRv}_{fit} - \mathrm{NIRv}_t)/(\mathrm{NIRv}_{t+1} - \mathrm{NIRv}_{t-1}) > 2$, and $\mathrm{NIRv}_{fit} > \mathrm{NIRv}_t$, where the subscript t is a time index, and NIRv_{fit} is the linearly interpolated NIRv between $t-1$ and $t+1$ (Bolton et al., 2020). Second, gaps in NIRvP during the spring leaf-out and autumnal senescence period were filled by borrowing observations from neighbouring years. This module was based on Bolton et al. (2020), though also similar to Jönsson et al. (2018) in that the data was first screened for gaps. Weights were assigned to neighbouring year observations according to Bolton et al. (2020), based on the similarity of NIRvP spline-fits in the gap-free window. Gap-filling was not extended to the middle of the growth season due to greater interannual variability in NIRvP at maturaity than during the leaf-out and senescence periods. Rather, NIRvP for the entire year was removed if the number of observations in June–August was less than two.

The image processing thus far resulted in a synthetic stack of daily NIRvP images for every year. For assessing year-to-year patterns of NIRvP, this information was condensed by calculating the growing season integrated NIRvP as the daily sum from May to mid October. The bounds of integration were shrunk if NIRvP rose (fell) above (below) zero before the hard-coded start (end) of season. This occurred mostly in years with late (early) spring (autumn) snowfall. The late summer NIRvP, which was calculated as the average NIRvP in mid July to August, was also assessed. This time window approximated the dry season when cottonwoods in the study area are most vulnerable to drought stress (Rood et al., 1995, 2003).

2.4 Remote sensing validation data

2.4.1 Ecosystem gas exchange

The eddy covariance technique was used to measure the net ecosystem carbon dioxide exchange (NEE) of the cottonwood forest within the HSNR at half-hourly intervals, from which rates of gross primary production (GPP) were derived. A 22 m tall telescoping tower that extended above the cottonwood canopy was instrumented during the growing season months. Measurements from four growing seasons were used; data from 2014, 2015, and 2017 have been previously published (Flanagan et al., 2017; Yang et al., 2019) and measurements from 2018 (June–September) were processed according to Flanagan et al. (2017). Details on the instrumentation, data processing, ancillary measurements, and derivation of GPP from NEE have been described elsewhere (Flanagan et al., 2017). Gap-filled half-hourly GPP were aggregated to daily totals for further analysis, with the exception of two periods in 2014 that data were completely gap-filled, due to evacuation of the field site during overbank flooding and an instrument failure; these data were discarded for the purpose of validating NIRvP.

2.4.2 Tree growth

Annual cottonwood trunk growth was derived from tree rings collected within the HSNR in 2009. Tree cores were collected from apparently healthy male and female narrowleaf cottonwoods ($n = 31$, combined) and radial increments (RI) and basal area increments (BAI) were calculated for years 1992–2008. Growth increments were averaged over all trees. These data have been previously published, and details on the sampling have been described elsewhere (Rood et al., 2013). Due to tree carbon allocation effects and different seasonal timing of leaf and trunk growth, comparison of NIRvP with growth increments was treated as a secondary validation—though some coordination was expected.

2.5 Historical climate and streamflow data

Daily minimum and maximum air temperatures and precipitation, aggregated to monthly values, were obtained from the Daymet Version 4 model output (Thornton et al., 1997), accessed from the Google Earth Engine. Daymet data were available 1984–2020. Temperature and precipitation data were used to calculate a simple soil moisture index (SMI) following Hogg et al. (2013), which represented the moisture held within a soil slab containing the upper 1.5 m of the subsurface. The SMI was a representation of relatively shallow soil moisture controlled solely by fluctuations in climate, rather than moisture held within the entire root zone, which would require information on alluvial groundwater table fluctuations and associated drainage and capillary fluxes to predict. 1980–1983 Daymet data were used as model spin-up.

Daily river discharges were accessed from the Water Survey of Canada website (`https://wateroffice.ec.gc.ca/`). Flows along the Lethbridge Reach were recorded at a gauging station about half a kilometer downstream of the HSNR. Flows along the Brocket Reach were estimated by adding flows from Pincher Creek (station 05AA033) to flows from the Oldman River near Brocket (05AA024), and flows along the Fort Macleod Reach were estimated by further subtracting the diversion at the LNID Weir (05AB019). The contribution of inflow from Willow Creek on streamflow towards the end of the Fort Macleod Reach was not included. Flows from the Crowsnest River (05AA008) were used to illustrate a free-flowing headwater catchment. Streamflow data were available 1984–2019 for the Lethbridge Reach, and 1984–2018 for the Brocket and Fort Macleod Reaches with gaps in 1995 and 2017 that were discarded, rather than filled.

2.6 Analysis

To validate NIRvP against GPP, cubic-spline fits of NIRvP were spatially averaged over a forest patch within the HSNR that aligned with the source area of the measured

turbulent fluxes, i.e. the flux footprint. Choosing the satellite image pixels to sample was guided by previous estimates of the flux footprint dimensions, after removing wind sectors with fetches that extended into an adjacent grassland (Flanagan et al., 2017). These pixels were used for the remainder of the study. Daily NIRvP and GPP were aggregated to weekly averages for meaningful comparison (Badgley et al., 2019). For validation of NIRvP against annual cottonwood growth, the growing season integrated NIRvP was used. The location of cored trees fell within the vicinity of the NIRvP source area. The correspondence between NIRvP and indicators of primary production were assessed using the coefficient of determination (r^2).

To illustrate year-to-year differences in NIRvP, seasonal courses were compared between select years. The growing season integrated or late summer NIRvP were otherwise assessed. Long-term changes in NIRvP were assessed by testing for a monotonic trend using the Mann-Kendall test, following steps recommended by Yue et al. (2002) to account for autocorrelation. For consistency, these steps were taken regardless of whether or not lag-one autocorrelation was statistically significant in the time series. The trend magnitude was estimated using the Theil-Sen estimator. NIRvP was standardized by dividing by the 1984–2020 average to allow for comparison of NIRvP between reaches, i.e. spatial differences in the magnitude of NIRvP were not considered. Statistical significance of trends were assessed at the 5% level.

The relationship between year-to-year NIRvP and environmental variables were assessed in an exploratory manner using Spearman's rank correlation coefficient (ρ_s). Attention was paid to possible pre- and post-dam differences, though rigorous assessment was difficult given the short pre-dam record. Different averaging schemes were tested on environmental variables, including seasonal and lagged averages. To test whether combinations of environmental variables were meaningful in explaining variation in NIRvP and to elucidate what variables were important for interpreting its long-term patterns, multiple linear regression models were built in a forward-

stepwise manner (*stepwiselm* function in MATLAB). Two sets of predictor variables were tested. The first applied the averaging schemes that yielded the strongest correlations with NIRvP in the exploratory analysis. The second assumed averaging schemes of October–April (dormant season), May–June (early growing season), and July–September (late growing season), including previous growing season conditions. Predictor variables were converted to z-scores so that model coefficients could be compared to assess predictor importance. The two-variable model that minimized the sum of squared errors was reported.

Chapter 3

Results

3.1 Historical climate and streamflow

The 1984–2020 study period displayed large interannual variability in streamflow and weather during the core growing season months along the Lethbridge Reach (Figure 3.1). From year-to-year, May–September streamflow ranged from 21 m^3 s^{-1} in 1988 to 266 m^3 s^{-1} in 1995 (average 107.8 m^3 s^{-1}), precipitation ranged from 56 mm in 2001 to 457 mm in 2005 (average 224 mm), and temperature ranged from 13.4 in 2010 °C to 16.8 °C in 1998 (average 15.3 °C). Moving averages showed that low flows occurred in several phases, approximately 1984–1989, 1999–2001, 2015–2019, and were separated by periods of variable, normal, or high flows. There tended to be an association between low (high) streamflow and dry (moist) climate conditions in the prairie region. Indeed, there was a correspondence between streamflow and the SMI during the growing season ($r^2 = 0.66$).

The most extreme streamflow anomalies occurred in drought and flood years. Low flows reflected both naturally low streamflow generation and elevated offstream diversion, due to higher irrigation demands from coincident dry atmospheric conditions. Notable low flow years included several years during the 1980's, particularly the warm summer of 1988 and 2000–2001, which experienced the lowest growing season precipitation during the study period. Major overbank flooding occurred along the Oldman River during the one-in-one hundred year flood in 1995 and again in 2013 and 2014; flooding in 2013 was widespread only along the Brocket and Fort Macleod Reaches.

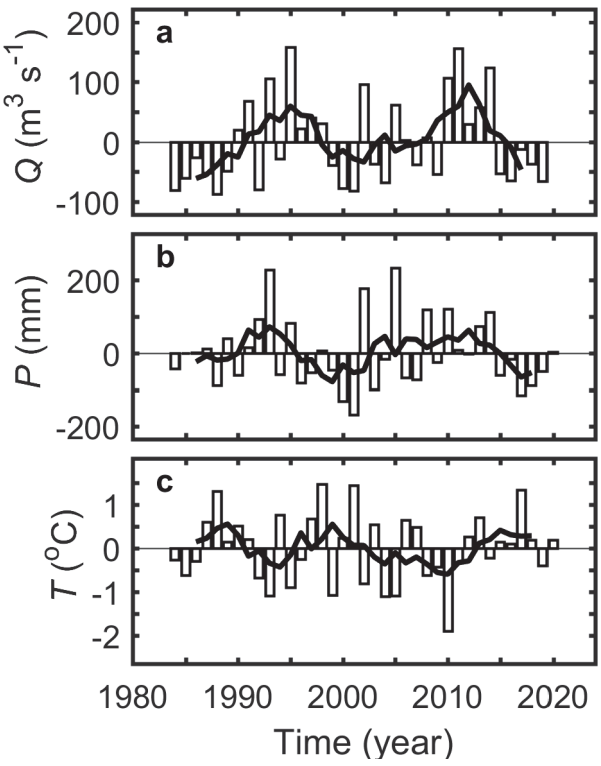

Figure 3.1: Anomalies of May–September (a) streamflow (Q), (b) precipitation (P), and (c) air temperature (T) along the Lethbridge Reach from 1984 to 2020. Bars are departures from the 1984–2020 average and lines are five year moving averages.

While spring storms are a prerequisite for floods along the Oldman River, high growing season precipitation in years such as 1993, 2002, or 2005 were not necessarily associated with floods, demonstrating the importance of timing and antecedent basin conditions.

3.2 Seasonal patterns of NIRvP

Seasonal courses of NIRvP at the HSNR were consistent with the foliar phenology of cottonwoods (Figure 3.2). Interannual variability in NIRvP was lowest during leaf-out and autumnal senescence in May and October, respectively, and greatest during the months that the canopy was at peak maturity, with up to two-fold differences between years. The radiation constraint was expected to introduce some year-to-year consistency to the seasonal pattern. A comparison of NIRvP during contrasting flood

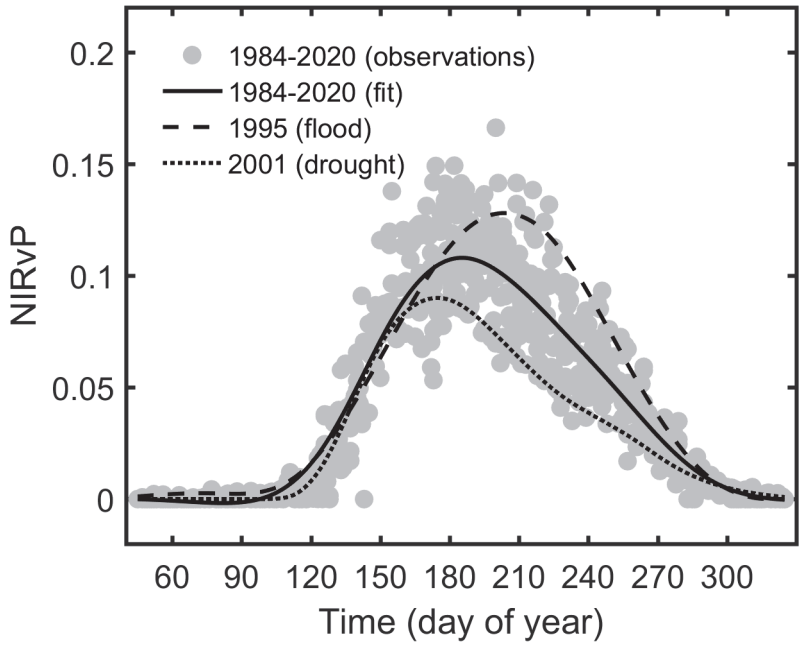

Figure 3.2: Comparison of the seasonal pattern of NIRvP during flood and drought years to average conditions at the Helen Schuler Nature Reserve. Points are a composite of all observations and lines are cubic spline-fits.

and drought years supported that interannual variability was associated with changes in weather, climate, and streamflow conditions. In the 2001 drought year, NIRvP was depressed throughout the growing season, particularly during the late summer months of July and August. In the 1995 flood year, NIRvP had a higher amplitude and seasonally accumulated value. The greatest difference between years was in the late summer. NIRvP was not necessary elevated in June of the flood year, when overbank flooding and associated wet and cool weather occurred.

A comparison of NIRvP during the 1988 and 2001 drought years revealed similar seasonal patterns (Figure 3.3). In 1988, mid–late summer flows were severely depleted, while flows were three times greater in 2001—though still greatly lacking relative to the average condition. Sustained mid–late summer flows in 2001 were compromised by some reduction of spring flows. As a result, the average growing season streamflow was similar between the two years (21 m^3 s^{-1} in 1988 and 26 m^3 s^{-1} in 2001). NIRvP

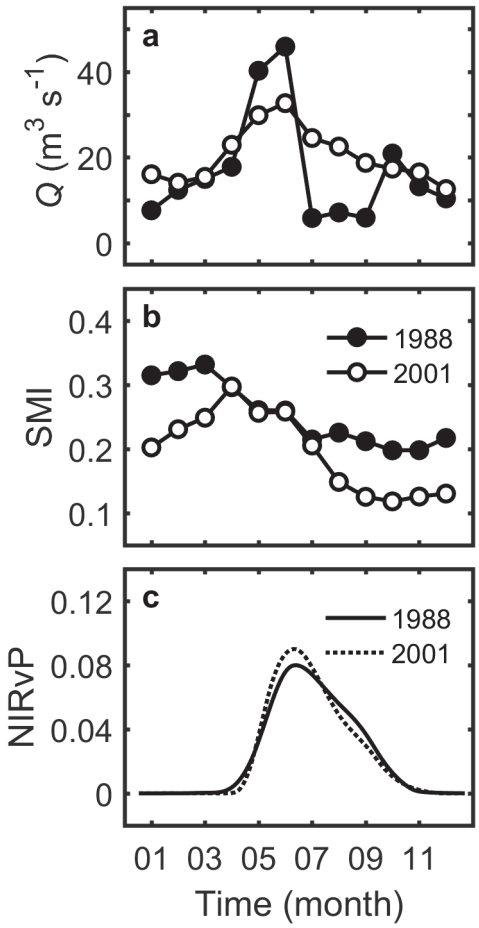

Figure 3.3: Seasonal patterns of (a) streamflow (Q), (b) a soil moisture index (SMI), and (c) cubic-spline fits of NIRvP during two drought years at the Helen Schuler Nature Reserve.

did not apparently respond to the extreme low flow condition in 1988. Rather, late summer NIRvP was slightly more depressed in 2001, in-line with the greater rate of shallow soil moisture depletion based on the SMI.

Parallel patterns of NIRvP and GPP were observed at the HSNR across the four years that the two data records overlapped (Figure 3.4). These were years of variable environmental conditions; 2014 was a flood year and the rest experienced low–average precipitation and streamflow (Figure 3.1; Yang et al. 2019). With weekly averaging, changes in GPP were gradual, reflecting convergent adjustments in canopy structure and carbon fixation capacity, rather than day-to-day fluctuations in weather. 2015 was somewhat of an exception, which may have been due to complex environmental conditions onset by episodes of wildfire smoke. Similar to NIRvP, GPP rose in May with expansion of the cottonwood canopy. Variable GPP at the beginning of May reflected different timing in the greening of grasses, forbs, and shrubs that occupied the forest understory. Peak GPP occurred in late June and early July when the canopy had fully expanded, days were the longest, and the recession of streamflow and onset of dry atmospheric conditions were only early underway. Throughout the remainder of the growing season, GPP and NIRvP declined progressively, and GPP returned to early May values with nearing autumnal senescence. The timing and rate of these declines fell between the two extremes illustrated previously with NIRvP (Figure 3.2). In 2014 and 2015, there was notable hysteresis between NIRvP and GPP, such that the decline of GPP in the late growing season preceded NIRvP.

NIRvP explained 85% of the variance in GPP at a weekly timescale, when observations were pooled across the four years (Figure 3.5). The relationship between the two was linear, with no sign of saturation at high values, and the intersection of the regression line near the origin reflected the adjustment made to account for non-zero NIRv during the dormant season. Hysteresis in 2014 and 2015 caused NIRvP to over-represent GPP by ca. 20%, across all growing season months, relative to the other

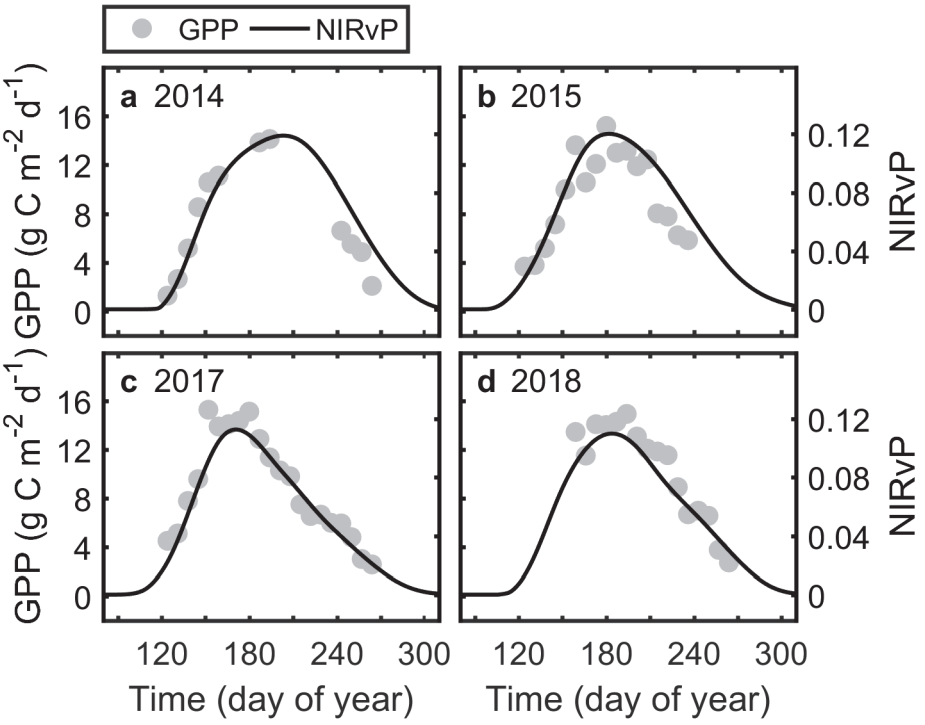

Figure 3.4: Seasonal courses of gross primary production (GPP) and NIRvP at the Helen Schuler Nature Reserve for (a) 2014, (b) 2015, (c) 2017, and (d) 2018. GPP are weekly averages and NIRvP are cubic-spline fits representing daily values. Y-axes are scaled to align with the ordinary regression line fitted through all years (Figure 3.5).

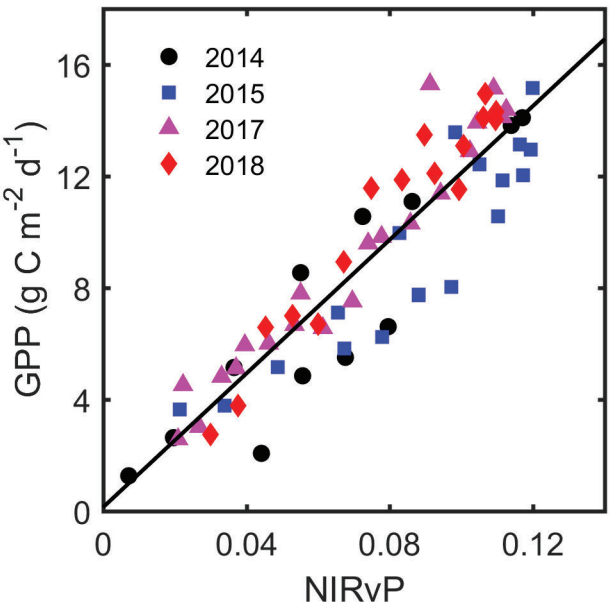

Figure 3.5: Relationship between weekly average NIRvP and gross primary production (GPP) at the Helen Schuler Nature Reserve across four years. The solid line is the ordinary regression line GPP = 119.9NIRvP + 0.14.

two years. Without the radiation constraint, NIRv explained 70% of the variance in GPP, hysteresis loops were wider, and there was some saturation of NIRv at high GPP (data not shown).

3.3 Long-term patterns of NIRvP

At the HSNR, which represented the heavily allocated Lethbirdge Reach, there was neither a long-term trend in the growing season integrated NIRvP (0.012 decade^{-1}, $p = 0.84$) nor the late summer NIRvP (0.044 decade^{-1}, $p = 0.50$) across the 1984–2020 study period. However, both measures displayed interannual variability that was associated with variation in streamflow, in most years (Figure 3.6). Specifically, the growing season NIRvP tracked lagged two-year (current and previous) flows, and the late summer NIRvP tracked June–August flows. Rather than comparing NIRvP to the generic pattern of growing season streamflow (Figure 3.1), strategic averaging schemes were applied based on exploratory analyses presented in Section 3.5.

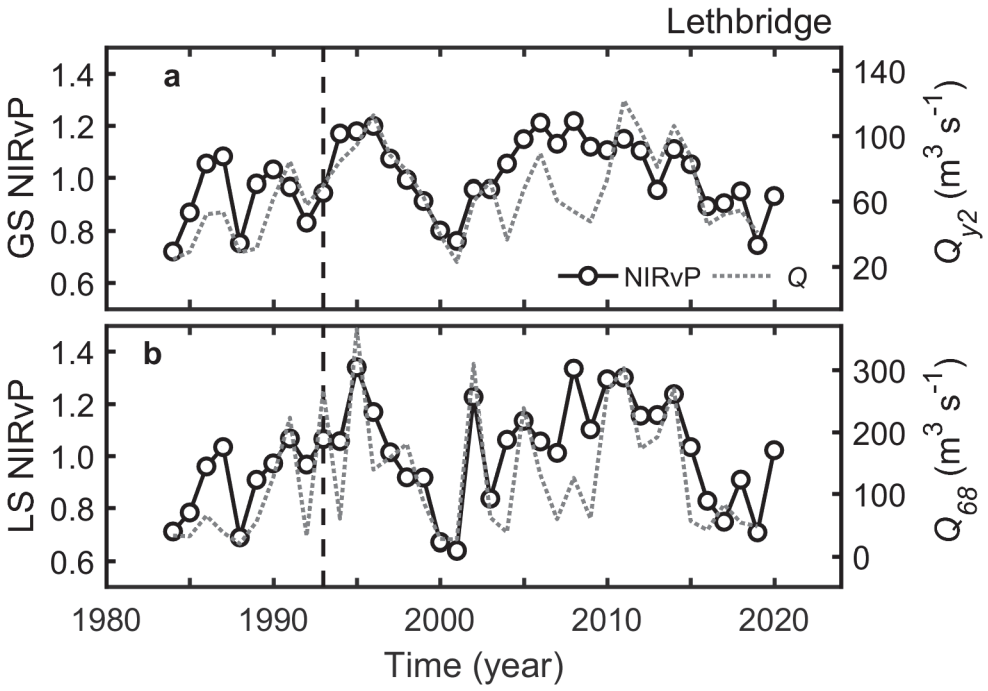

Figure 3.6: NIRvP and streamflow along the Lethbridge Reach from 1984 to 2020. (a) Growing season integrated (GS) NIRvP and previous–current year streamflow (Q_{y2}). (b) Late summer (LS) NIRvP and June–August streamflow (Q_{68}). NIRvP was standardized by dividing by the 1984–2020 mean. The dashed vertical line marks the completion of the Oldman River Dam in 1993.

Patterns of the growing season integrated NIRvP and the late summer NIRvP were similar, though the latter was more dispersed and less serially correlated. In pre-dam years, NIRvP was low–average, reflecting climate and streamflow conditions. Although this period contained some of the lowest NIRvP years, NIRvP was not reflective of severe dewatering that was re-occurring during the mid–late summer months (Figure 2.2). NIRvP promptly recovered from low flow years such as 1984 and 1988 with return of average streamflow conditions, resulting in mismatches between the growing season integrated NIRvP and lagged two-year flows in the following year. In post-dam years, NIRvP was variable; lows were associated with the 2000–2001 drought and recent dry years, while highs were associated with wet years—not necessarily flood years. Highs in the growing season integrated NIRvP were also associated with wet conditions in the previous year. In 1994, for example, which was a year of

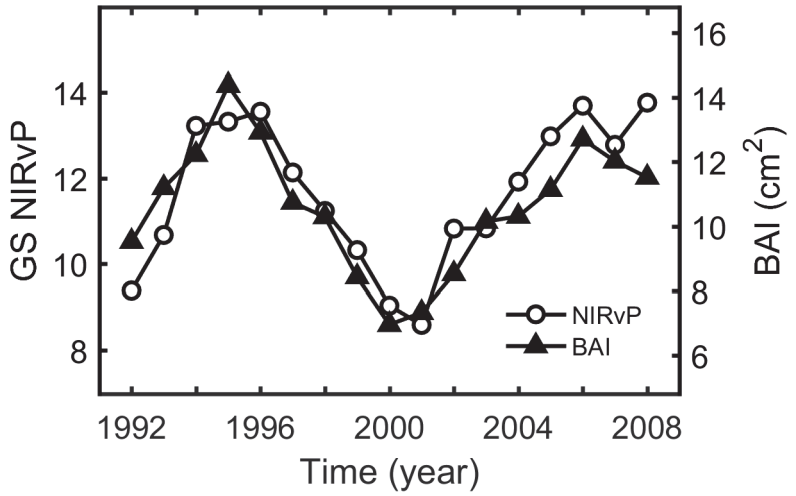

Figure 3.7: Growing season integrated (GS) NIRvP and cottonwood basal area increments (BAI) at the Helen Schuler Nature Reserve from 1992 to 2008.

average environmental conditions, NIRvP was elevated, appearing to respond to high flows and precipitation in 1993.

Cottonwood RI and BAI during the 1992–2008 period at the HSNR generally followed the same trajectory as the growing season integrated NIRvP, dipping to a minimum during the 2000–2001 drought and recovering in subsequent years (Figure 3.7; RI data shown in Rood et al. 2013). The pattern of recovery was less pronounced for growth increments. The growing season NIRvP explained 55% and 78% of the variance in RI and BAI, respectively. Without the radiation constraint, NIRv explained 54% and 74% of the variance, respectively.

3.4 Spatial patterns

Among the three study reaches, there was high correspondence in growing season streamflow ($r^2 > 0.89$) and climate conditions ($r^2 > 0.85$). Thus, relative year-to-year patterns described for the Lethbridge Reach (Section 3.1) were applicable elsewhere. However, the magnitude of the year-to-year variability was amplified downstream, due to greater offstream diversion in dry years. A comparison of hydrographs among

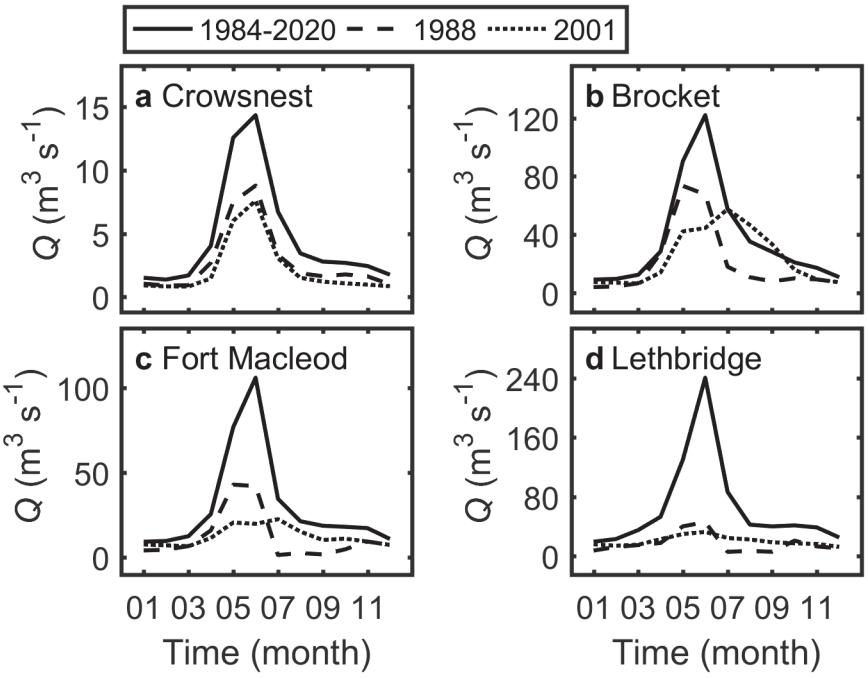

Figure 3.8: Seasonal streamflow (Q) for the (a) free-flowing Crowsnest River and the (b) Brocket, (c) Fort Macleod, and (d) Lethbridge Reaches of the Oldman River during two drought years, compared to the 1984–2020 average.

reaches during the 1988 and 2001 drought years illustrated this point, with runoff progressively decreasing downstream relative to average conditions (Figure 3.8). An exception to this pattern was 1992, when initial filling of the Oldman River Reservoir reduced flows more strongly along the Brocket and Fort MacLeod Reaches than the Lethbridge Reach, which was alleviated by inflows from the Belly and St. Mary Rivers. The comparison of hydrographs also illustrated the effects of river regulation and management. Along the Fort Macleod and Brocket Reaches, enhanced minimum flow requirements restored streamflow during the mid–late summer in the post-dam year. However, this was met with some reservoir trapping of peak flows during the spring. Along the Brocket Reach, reservoir storage effects were pronounced in the post-dam year, while the pre-dam hydrograph reflected the free-flowing Crowsnest River. In terms of climate conditions, the SMI confirmed increasing aridity further from the foothills (Figure 3.9)

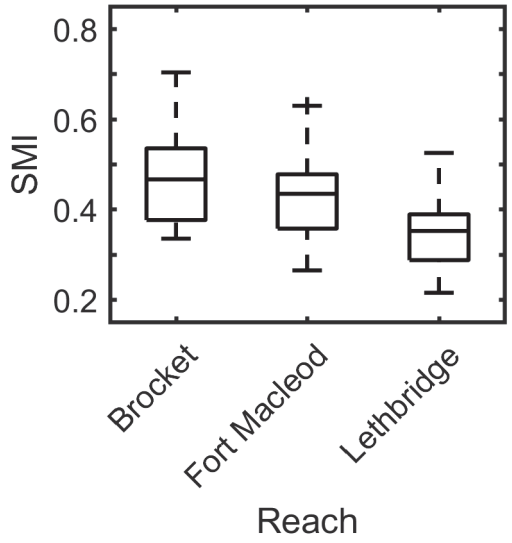

Figure 3.9: Boxplots of May–September soil moisture index (SMI) along the Lethbridge, Fort Macleod, and Brocket Reaches of the Oldman River from 1984 to 2020.

NIRvP along the Fort Macleod and Brocket Reaches did not contain long-term trends (summarized in Table 3.1), but generally tracked year-to-year streamflow (Figures 3.10, 3.11). Patterns of NIRvP along both reaches were less variable than the Lethbridge Reach, consistent with spatial differences interannual streamflow variability. In pre-dam years, NIRvP along the Fort Macleod Reach was comparable to the then-free-flowing Brocket Reach, despite the diversion at the LNID Weir. Both reaches showed modest values of NIRvP during the pre-dam period relative to the Lethbridge Reach, especially in years such as 1988. Rather, the pre-dam year with the lowest NIRvP was the 1992 reservoir filling year, particularly for the growing season integrated NIRvP. In post-dam years, neither reach responded as positively

Table 3.1: Trends (relative to the mean) in the growing season integrated (GS) and late summer (LS) NIRvP along three reaches of the Oldman River between 1984 and 2020.

Reach	GS trend (decade^{-1})	p-value	LS trend (decade^{-1})	p-value
Lethbridge	0.012	0.84	0.044	0.50
Fort Macleod	−0.006	0.24	0.001	0.92
Brocket	0.010	0.47	0.022	0.30

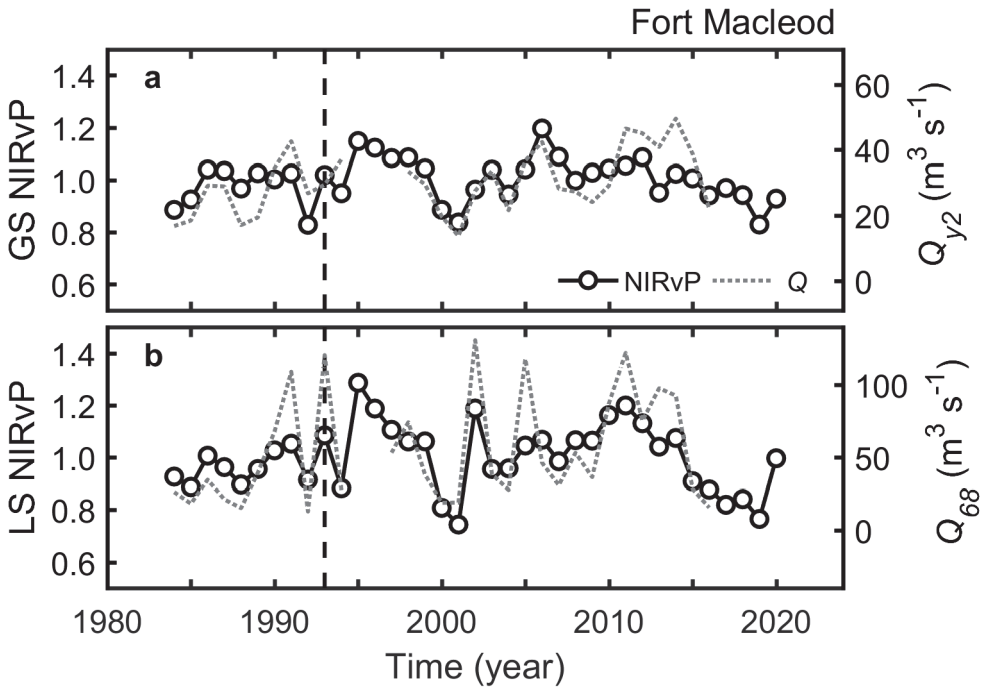

Figure 3.10: Same as Figure 3.6 but for the Fort Macleod Reach.

to the 1995 flood as the Lethbridge Reach. Both reaches declined to lows during the 2000–2001 drought and responded positively to the return of moisture in 2002. In the subsequent years, patterns of NIRvP and streamflow along both reaches were synchronous until the wet 2010–2014 period.

On a pixel basis, 16% and 14% of the Fort Macleod and Brocket Reaches combined showed significant positive and negative trends, respectively, in the growing season integrated NIRvP (Figures 3.12, 3.13). Along the Fort Macleod Reach, there were both patchy declines in NIRvP, such as along the southern-most portion of the reach through the Town of Fort Macleod, and uniform declines restricted to single groves, such as a cluster of point bars and islands within a braided segment of the reach. The spatial behavior of positive change pixels were similar. Along the Brocket reach, spatial patterns appeared more variable. However, extraction of historical surface water extent using the Landsat quality assessment band revealed some association between change pixels and channel migration (Figure 3.13). Specifically, positive

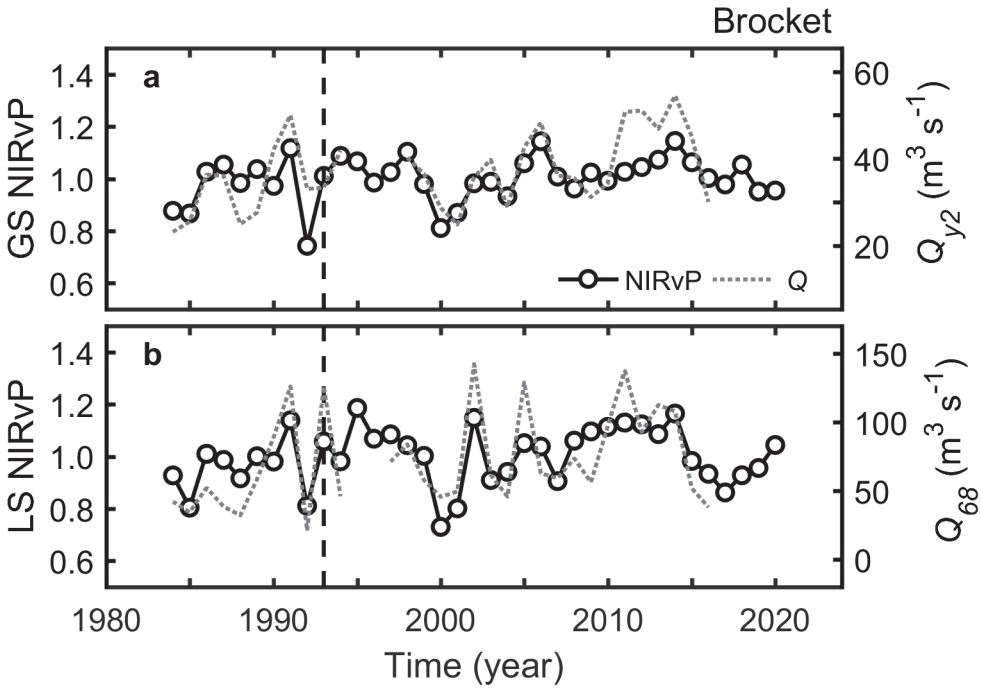

Figure 3.11: Same as Figure 3.6 but for the Brocket Reach.

(negative) trends were associated with channel segments that migrated towards (away from) those forest patches. Channel migration was primarily associated with the 2013 flood, although some precedent shifts appeared to be underway following high flows in 2005, based on historical Landsat images. There were also some negative change pixels associated with floodplain positions furthest away from the active channel.

3.5 Relationships between NIRvP and environmental variables

Correlation analysis of NIRvP with growing season environmental variables showed that NIRvP was more strongly correlated with streamflow and the SMI than with precipitation and temperature, and that the late summer NIRvP was more responsive than the growing season integrated NIRvP (Table 3.2). Correlation strengths with streamflow and precipitation were consistent across the three reaches, but for temperature and the SMI, they increased further from the foothills.

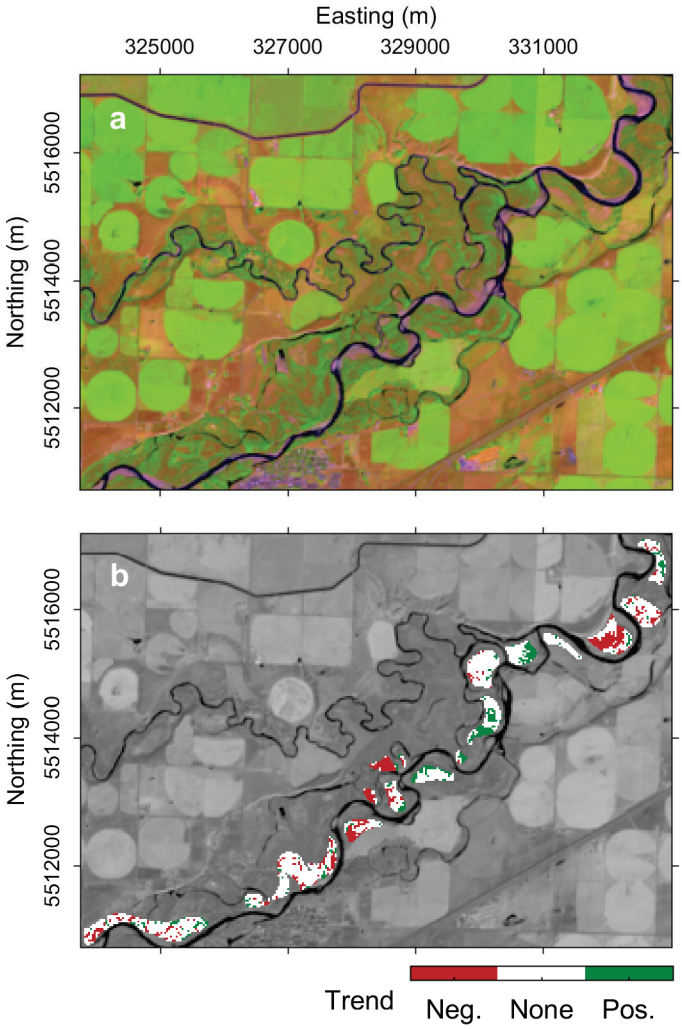

Figure 3.12: (a) Landsat 8 false colour composite image (SWIR1/NIR/G) of the Fort Macleod Reach. (b) Trend image for the growing season integrated NIRvP from 1984 to 2020. The background image is the composite from (a) in grayscale for spatial reference. Northings and eastings are for UTM zone 12.

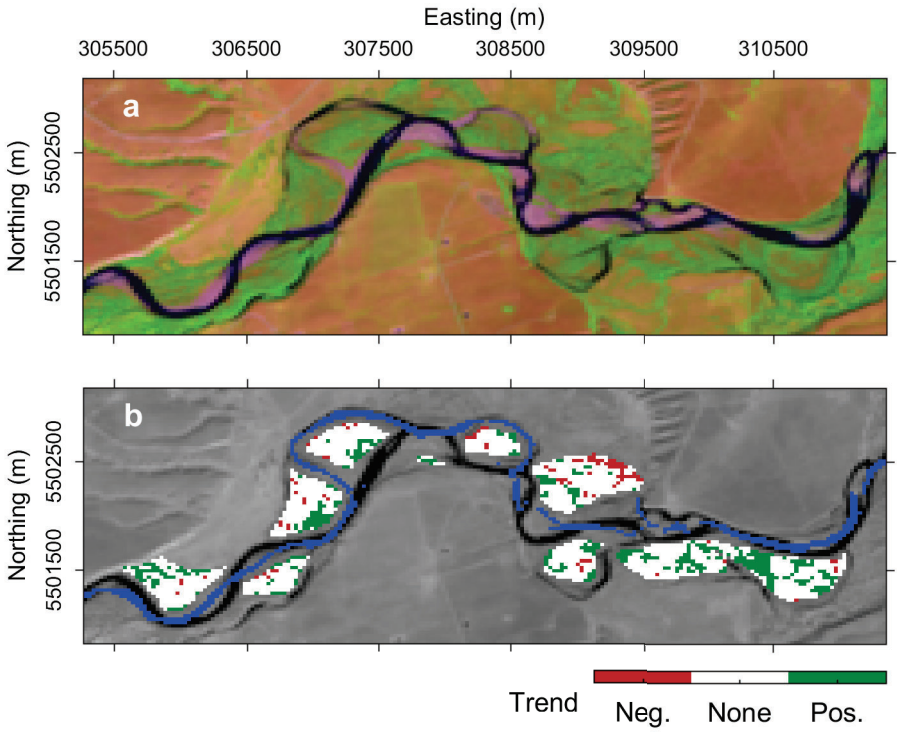

Figure 3.13: (a) Landsat 8 false colour composite image (SWIR1/NIR/G) of the Brocket Reach. (b) Trend image for the growing season integrated NIRvP from 1984 to 2020. The background image is the composite from (a) in grayscale for spatial reference and an estimate of the active river channel extent from 1984 to 2012 is illustrated in blue. Northings and eastings are for UTM zone 12.

Table 3.2: Spearman's rank correlation coefficients (ρ_s) between the growing season integrated (GS) NIRvP or the late summer (LS) NIRvP and May–September streamflow (Q_{59}), temperature (T_{59}), precipitation (P_{59}), or soil moisture index (SMI_{59}) along three reaches of the Oldman River. Asterisks denote the following levels of significance: $p < 0.01$ (***), $p < 0.05$ (**), $p < 0.10$ (*).

Reach	NIRvP metric	ρ_s			
		Q_{59}	P_{59}	T_{59}	SMI_{59}
Lethbridge	GS	0.58^{***}	0.25	-0.11	0.69^{***}
	LS	0.77^{***}	0.63^{***}	-0.40^{**}	0.81^{***}
Fort Macleod	GS	0.53^{***}	0.09	0.05	0.61^{***}
	LS	0.78^{***}	0.51^{***}	-0.33^{**}	0.77^{***}
Brocket	GS	0.54^{***}	0.17	0.26	0.48^{***}
	LS	0.78^{***}	0.55^{***}	-0.27	0.66^{***}

For the growing season integrated NIRvP, correlation strengths with environmental variables were enhanced when either restricting averaging to May–June, or incorporating information on prior conditions. Prior dormant and growing season information enhanced correlation strengths with streamflow, with lagged two-year (current and previous) flows yielding the strongest correlations across reaches ($\rho_s = 0.57$–0.73; Figure 3.14). Averaging from the previous May to current June yielded the strongest correlations with precipitation ($\rho_s = 0.48$–0.65; Figure B.1), but correlation strengths were outperformed by May–June SMI, except for the Brocket Reach ($\rho_s = 0.43$–0.73; Figure 3.14). Lagged SMI did not enhance correlation strengths. May–June maximum temperature was negatively correlated with the growing season NIRvP, only for the Lethbridge and Fort Macleod Reaches ($\rho_s = -0.41 - -0.34$). For the late summer NIRvP, narrowing the averaging window to the corresponding months of July and August was not necessarily advantageous; the change in correlation strength was negligible for temperature and only slightly positive for SMI, but negative for precipitation and streamflow. Rather, a June–August window yielded the strongest correlations with streamflow ($\rho_s = 0.79$–0.84; Figure 3.15). This was a slight improvement to the generic May–September window, which was ideal for precipitation and temperature (Table 3.2; Figure B.1). Between pre- and post-dam periods, there

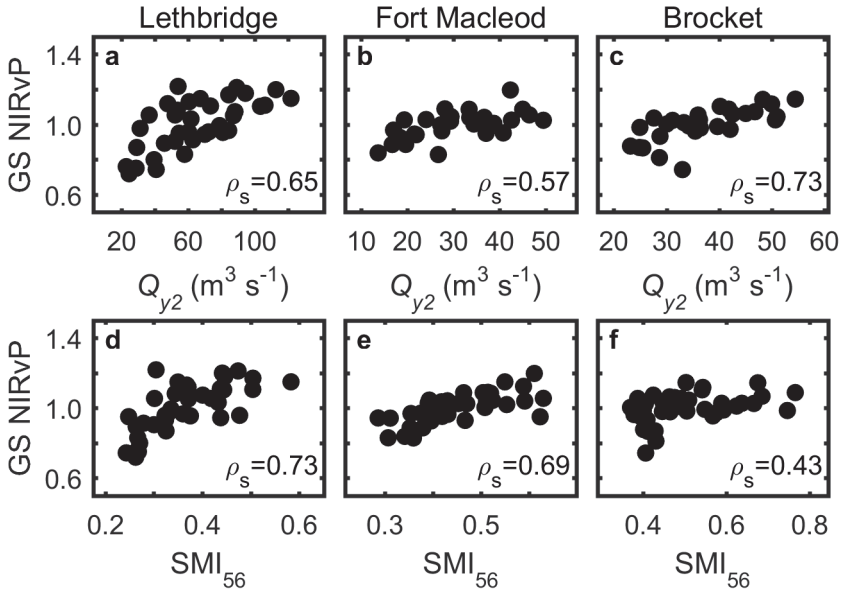

Figure 3.14: Relationships between the growing season integrated (GS) NIRvP and (a,b,c) previous–current year streamflow (Q_{y2}) or (d,e,f) May–June average soil moisture (SMI_{56}) along the (a,d) Lethbridge, (b,e) Fort Macleod, and (c,f) Brocket Reaches. Spearman's rank correlation coefficients (ρ_s) are noted.

were no apparent differences in the correlation between NIRvP and environmental variables, nor the shape of their relationship.

SMI not only was a stronger correlate of NIRvP than precipitation, but, in some cases, even outperformed streamflow in correlation strength, such as along the Lethbridge Reach (Figures 3.14, 3.15). After applying the best averaging schemes, year-to-year patterns of streamflow and the SMI were similar along the Lethbridge Reach (Figure 3.6, 3.16). Their patterns of synchrony and asynchrony with NIRvP were comparable, yet the SMI outperformed streamflow in pre-dam years.

Streamflow and the SMI were the two variables exclusively selected into linear models predicting NIRvP. In the first set of models, which applied the most successful averaging schemes from the correlation analysis to predictor variables, only one of streamflow or the SMI was selected. Thus, their predictive power was similar. In the second set of linear models, which were built from seasonally averaged predictor variables (Table 3.3), May–June streamflow or SMI tended to be selected as the most

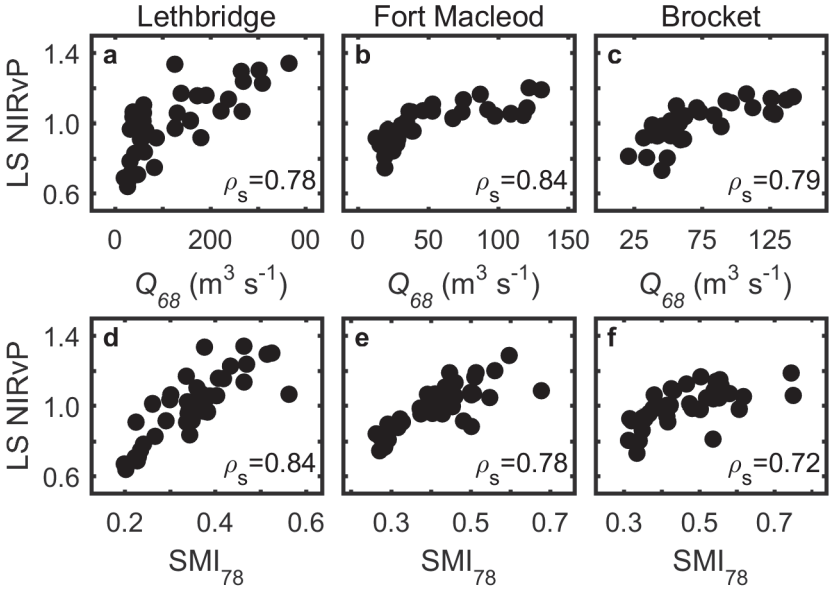

Figure 3.15: Relationships between the late summer (LS) NIRvP and (a,b,c) Jun–Aug streamflow (Q_{68}) or (d,e,f) July–August average soil moisture index (SMI_{78}) along the (a,d) Lethbridge, (b,e) Fort Macleod, and (c,f) Brocket Reaches. Spearman's rank correlation coefficients (ρ_s) are noted.

important predictor variable, followed by prior moisture conditions, for the growing season integrated NIRvP. The most important predictor for the late summer NIRvP was July–September SMI along the Lethbridge Reach, and May–June streamflow along the Fort Macleod and Brocket Reaches, followed by either moisture conditions in the prior year or the late growing season months. The percentage of the variance in NIRvP explained by the two parameter models was higher for downstream reaches further from the foothills.

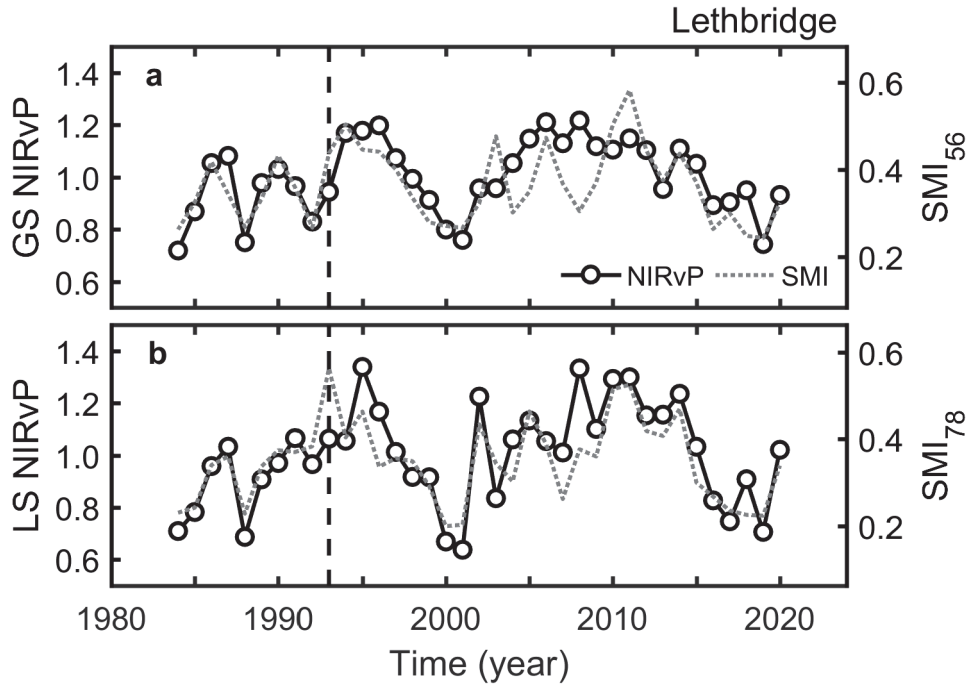

Figure 3.16: NIRvP and a soil moisture index (SMI) along the Lethbridge Reach from 1984 to 2020. (a) Growing season integrated (GS) NIRvP and May–June SMI (SMI_{56}). (b) Late summer (LS) NIRvP and July–August SMI (SMI_{78}). NIRvP was standardized by dividing by the 1984–2020 mean. The dashed vertical line marks the completion of the Oldman River Dam in 1993.

Table 3.3: Model selection from stepwise linear regression predicting either the growing season integrated (GS) NIRvP or the late summer (LS) NIRvP along three reaches of the Oldman River. Predictor variables, their coefficients (standardized) and associated p-values, as well as model coefficients of determination (r^2) are listed. Selected predictor variables are streamflow (Q) and a soil moisture index (SMI). Subscripts refer to the start and end month that a predictor variable is averaged over, where the appended subscript pr denotes that averaging begins and ends in those months of the prior year.

Reach	NIRvP metric	Predictor variable	Coefficient	p-value	r^2
Lethbridge	GS	SMI_{56}	0.080	< 0.01	0.54
		SMI_{56pr}	0.040	0.05	
Lethbridge	LS	SMI_{79}	0.138	< 0.01	0.77
		SMI_{56pr}	0.072	< 0.01	
Fort Macleod	GS	SMI_{56}	0.064	< 0.01	0.48
		Q_{79pr}	-0.027	0.03	
Fort Macleod	LS	Q_{56}	0.054	< 0.01	0.67
		SMI_{79}	0.046	0.01	
Brocket	GS	Q_{56}	0.049	< 0.01	0.44
		SMI_{104}	0.036	0.02	
Brocket	LS	Q_{56}	0.067	< 0.01	0.56
		Q_{79}	0.029	0.06	

Chapter 4

Discussion

4.1 Scaling primary production with NIRvP

The strong correlation of NIRvP with both GPP and annual cottonwood growth in a native riparian forest showed that the canopy structural information contained in NIRvP provided a practical yet meaningful proxy of primary production for this ecosystem type (Figures 3.4, 3.5, 3.7). These results were necessary for reliable temporal scaling of productivity and accurate historical assessments of ecosystem health. Since the degree of variation in the NIRvP–GPP slope between spatial units was unknown, spatial assessments of productivity were not pursued. Specifically, it could not be ruled out that there was spatial variation in canopy architecture and physiology that would alter the coordination between canopy visible light absorption, near-infrared light scattering, and photosynthetic capacity (Badgley et al., 2019; Baldocchi et al., 2020; Zeng et al., 2019). Similar dilemmas on the scaling of canopy structure to function have been noted for the estimation of riparian vegetation water use from satellite vegetation indices (Mayes et al., 2020), though networks of validation sites along river corridors have enhanced confidence in empirical predictions (Nagler et al., 2005).

The theoretical basis for NIRv as a proxy for GPP can be traced back to Sellers (1987), who showed that the reflectance of green vegetation to near-infrared light should scale near-linearly with its absorptance to visible light, based on the nature of the spectral properties of green leaves and their distribution in space within the

canopy. Sellers showed that the link to canopy visible light absorptance is typically satisfied using traditional remotely sensed vegetation indices, but is deteriorated by the contribution of soil to land surface reflectance. Thus, by aiming to disentangle the relative contributions of soil and vegetation to total scene reflectance, NIRv represents a new solution to this old problem.

Remotely sensed structural proxies for primary production typically provide information on time-integrated rates of productivity over weeks–months, based on a functional convergence between canopy visible light absorptance and carbon fixation capacity (Badgley et al., 2019; Field, 1991). The ability for NIRv to be expressed in radiance units represents another advancement of NIRv over traditional vegetation indices (Baldocchi et al., 2020; Dechant et al., 2020; Wu et al., 2020). As a rate process, NIRv can resolve fluctuations in photosynthetic activity at shorter timescales, for example Wu et al. (2020) were able to track sub-daily rates of GPP over a corn and soybean crop using near-surface measurements of radiance-based NIRv. NIRvP, which scaled NIRv with potential irradiance in this study, represented an intermediate between reflectance- and radiance-based NIRv. While these two representations of NIRv may be different at short timescales, they tend to converge over weeks (Dechant et al., 2020; Wu et al., 2020). Indeed, at a weekly timescale, NIRv explained more of the variance in GPP with the radiation constraint than without, yet at an annual timescale the constraint did not considerably enhance the explained variance in cottonwood trunk growth. Thus, adding the radiation constraint improved the seasonal representation of GPP, but its effect on year-to-year patterns of productivity was small.

The scaling of NIRvP to GPP was generally consistent across four growing seasons at the HSNR, but there was a tendency for late summer declines in NIRvP to lag behind GPP in 2014 and 2015 (Figure 3.4). This was partly expected due to the slow versus fast response of canopy structure and photosynthetic activity, respectively, to

changes in the plant environment (Badgley et al., 2019). However, the absence of notable hysteresis in other validation years suggested that this temporal mismatch may have been dependent on the level and type of resource limitation or stress. Interestingly, hysteresis was associated with years of relatively high cottonwood moisture supply; 2014 was a flood year and in 2015 there was substantial carry-over of prior year moisture within the unsaturated zone that supplemented the low streamflow (Flanagan et al., 2017; Yang et al., 2019). If this association was indeed true, it would suggest that GPP was over-represented by NIRvP in wet years. However, NIRvP would still have been expected to track the directional response of productivity to year-to-year moisture availability; the caveat would have been that NIRvP was less sensitive to other resource limitations or stresses in years that moisture was abundant.

Records of annual cottonwood growth extended the scope of the remote sensing validation in terms of both temporal and biological scale. First, the correspondence between NIRvP and BAI—and less-so RI—provided direct evidence for the ability of NIRvP to track year-to-year differences in productivity. This alleviated some concern that arose from the validation of NIRvP against the relatively short GPP record. Second, the correspondence confirmed that productivity at the ecosystem-scale reflected productivity of the cottonwood population. This result was important because NIRvP represented a combined spectral signal from the cottonwood canopy and a community of grasses, forbs, and shrubs that were visible to the satellite sensor from gaps in the tree canopy. At the HSNR, this mostly herbaceous understory community contributed to half of the ecosystem leaf area index (1.8 m^2 m^{-2} in a wet year, Flanagan et al. 2017). On one hand, the herbaceous community contributes to the ecosystem's ecological diversity, including functions that are likely beneficial for cottonwoods such as mineral nutrient input into the shallow soil. On the other hand, spectral mixtures can confine assessments of health. For example, Gómez-Sapiens et al. (2020) found that elevated vegetation greenness following an environmental pulse flow reflected en-

hanced productivity of emergent wetland species rather than riparian trees. Their recommendation that ecosystem-scale validation of remotely sensed proxies should be complimented with species specific data is agreeable. While mixed pixels were inevitable with medium spatial resolution imagery, these results suggested that their contribution was small, or there was co-variation in the productivity of cottonwoods and the herbaceous community.

4.2 Moisture dependency of riparian forests

With limited precipitation in semi-arid climates, riparian cottonwoods are reliant on alluvial groundwater to meet their water requirements (Rood et al., 2003). Along the Oldman River, this is evidenced by observations of root structures exposed at river cut-banks (Rood et al., 2011), growing season water use (Flanagan et al., 2017; Yang et al., 2019), and diurnal pulsing of alluvial groundwater tables (Rood et al., 2013). More widely documented, along various nival rivers across semi-arid and arid North America, is a correlation between cottonwood growth and streamflow (Andersen, 2016; McNeeley et al., 2020; Philipsen et al., 2018; Schook et al., 2020; Stromberg & Patten, 1990). The correlation of NIRvP with streamflow was consistent with these findings, however NIRvP was correlated with a climatic soil moisture index (SMI) to a similar extent (Figures 3.14, 3.15; Table 3.2). Did this reflect an association between streamflow and precipitation, or were cottonwoods also dependent on relatively shallow soil moisture? It could be argued that both factors likely contributed. On one hand, growing season climate conditions in the prairie region do tend to be associated with streamflow, which primarily reflects winter alpine precipitation (Figure 3.1; Rood et al. 2013). On the other hand, the intolerance of cottonwoods to inundation suggests that investing in root growth within multiple soil layers would be advantageous along seasonally dynamic nival rivers (Amlin & Rood, 2001; Rood et al., 2011). This would include both deep soil layers that fill and drain with the seasonal rise and fall of the

alluvial groundwater table, and shallow soil layers that escape seasonal inundation and offer a source of mineral nutrients from decomposition of deciduous litter (Rood et al., 2011; Williams & Cooper, 2005). Thus, infiltrating precipitation represents an important water input into the shallow root zone that is less frequently recharged by—or completely disconnected with—the water table. Indeed, at the HSNR, prior stable isotope work has shown that cottonwoods at this site do not rely exclusively on root zone water inputs from the alluvial groundwater table (Flanagan et al., 2019).

Correlation of cottonwood growth with both current and prior year flows has been noted by various workers and attributed with mechanisms such as utilization of stored prior-year assimilate and basin water storage (Andersen, 2016; Philipsen et al., 2018; Stromberg & Patten, 1990). Antecedent streamflow conditions were similarly important for NIRvP; prior year flows were important for the growing season integrated NIRvP, in addition to current year flows, and June flows were important for the late summer NIRvP, in addition to July–August flows. An interpretation of this finding is that lagged flows, which captured high flow periods either earlier in the growing season or in the prior year, provided information on root zone recharge. Measurements of soil volumetric water content within the upper 250 cm of the subsurface at the HSNR have shown that there is potential for substantial water storage in the unsaturated zone above the alluvial groundwater table (Flanagan et al., 2017; Yang et al., 2019). Thus, high flows recharging this reservoir would provide a water source for progressive uptake by cottonwoods throughout the growing season, supplementing direct uptake from the capillary fringe. High flows may also supplement root zone water inputs in the following year through water storage (Yang et al., 2019). Similarly, for precipitation, extending the averaging period to include the wettest months of May–June in the current or prior year provided information on recharge of the relatively shallow root zone.

Combining current and prior year streamflow to depict the root zone water balance

was not always successful. For example, available moisture was over-represented when high flow years occurred in succession, due to neglected drainage, as was evident along the Fort Macleod and Brocket Reaches (Figures 3.10, 3.11). Along the Lethbridge Reach, it was also evident that lagged flows obscured prompt recoveries in NIRvP with return of adequate moisture conditions following low flow years (Figure 3.6). The SMI was not prone to these effects, since it explicitly tracked the water balance of a soil slab (Figure 3.16; Hogg et al. 2013). However, the SMI was only a partial representation of root zone moisture, since it did not account for alluvial groundwater table fluctuations and associated drainage and capillary fluxes. Although the abundance of moisture in the deep and shallow root zones probably co-varied in most years, mechanistically their combined contribution to ecosystem water source is consequential for productivity, particularly during periods that one is lacking (Hultine et al., 2010; Tai et al., 2018). Besides direct simulation of the variably saturated zone (Tai et al., 2018), ideally there is some simple parameterization for the effect of river flow fluctuations on root zone water storage that can be incorporated into an index like the SMI.

Since root zone water storage was implicit in the SMI, its correspondence with NIRvP would presumably have been temporally aligned, e.g. May–September SMI would have tracked the growing season integrated NIRvP. However, this was only true for the late summer NIRvP, as May–June SMI yielded the strongest correlation with the growing season integral. Phenology may explain the importance of early growing season conditions for NIRvP, since annual integrals of NIRvP would be dominated by their amplitudes (Field, 1991), which would be primarily reflections of conditions for photosynthetic activity during the spring when the canopy is being constructed. More generally, this points to a retrospective component of NIRvP that owes to the fact that canopy structure is largely a reflection of past rates of productivity (Field, 1991).

As shallow soil moisture became a less reliable water source further from the

foothills (Figure 3.9), cottonwoods were expected to increasingly rely on alluvial groundwater to thrive, investing in deeper root growth (Rood et al., 2011). On this basis, it was hypothesized that correlation strengths between NIRvP and streamflow would increase along the moisture gradient from foothills to prairies. However, consistently high correlation strengths across the three reaches did not support this hypothesis. Rather, correlation strengths between NIRvP and the SMI followed this spatial pattern (Table 3.2). This suggested that cottonwoods within the prairie region have similar functional rooting depths that tap deep soil layers recharged by the alluvial groundwater table, yet their shallow roots are increasingly moisture limited further from the foothills. The selected linear models supported this same spatial pattern of moisture limitation—though indiscriminate of the specific water source—based on their increasing predictive power downstream (Table 3.3). These findings offered empirical insight into how sensitive riparian forests were to year-to-year fluctuations in streamflow and climate (Mayes et al., 2020; Stromberg & Patten, 1990, 1996).

4.3 Impacts of river regulation and management

In terms of river regulation and management, the study period was divided by the Oldman River Dam Project and the collective adoption of functional flow regimes by dams basin-wide (Foster et al., 2018; Rood & Mahoney, 2000; Rood et al., 2005). In pre-dam years, cottonwoods were expected to have responded to unfavourable streamflow conditions during the dry mid–late summer months by reducing water loss and demand at the expense of curtailed carbon assimilation (Horton et al., 2001; Hultine et al., 2010; Rood et al., 2003; Smith et al., 1991). With revised dam operations, low flow conditions during the mid–late summer were naturalized (Figure 2.2), and cottonwoods were anticipated to respond positively with enhanced vigour. However, the satellite record did not offer any evidence of widespread restoration that would support this hypothesis, nor, conversely, evidence of widespread degradation.

Flow–productivity relationships were not fundamentally different between pre- and post-dam periods either. The apparent lack of response of riparian forests to revised dam operations was perhaps unsurprising, since year-to-year patterns of NIRvP were largely driven by high flow characteristics and peak flows that were responsible for recharging root zone moisture. There was also the role of phenology to consider—that is NIRvP may have primarily reflected how favourable conditions were for photosynthetic activity during the early growing season. Does this explain the apparent lack of response of NIRvP to severe dewatering during the mid–late summer months? Not necessarily, since stressful conditions during the late summer could have still manifested as losses in green canopy vigour in future growing seasons, either from a lack of resources to construct and maintain the green canopy, or directly from woody biomass losses associated with branch shedding or partial crown dieback (Hultine et al., 2010; Rood et al., 2000; Williams & Cooper, 2005).

In pre-dam years, cottonwoods likely avoided, resisted, and were resilient to drought-like conditions imposed by streamflow reductions during the mid–late summer months. The most unfavourable conditions persisted from 1977 to 1989, which was the combined result of water diversion and naturally low streamflow generation associated with the Pacific Decadal Oscillation (Figure 2.2; Rood & Vandersteen 2010). Although unfavourable conditions were re-occurring, they were seasonal, therefore not chronic. Presumably, root zone water storage adequately buffered cottonwoods against low alluvial groundwater tables. This would have owed to less severely depleted peak flows and average precipitation conditions that recharged root zone moisture between episodes of water table draw-down. These interpretations are in-line with results from a coupled plant hydraulics–hydrological model that showed root zone water storage to buffer cottonwoods against short-term reductions in streamflow (Tai et al., 2018). Cottonwoods in the study area are also likely adapted to thrive in the dry climate. Proxy records of climate and streamflow for the western Canadian prairies show that

drought severity and duration is not fully represented in instrument records (Axelson et al., 2009; Sauchyn & Skinner, 2001). Thus, streamflow conditions during the last half-decade may have been within the natural tolerance range of cottonwoods to drought stress. Optimal stomatal conductance, structural plasticity, and robust root structures, including diverse mycorrhizal associations, have likely allowed cottonwoods to cope with past drought cycles and recent river regulation (Hultine et al., 2020; Rood et al., 2000; Williams & Cooper, 2005). In terms of productivity, cottonwoods were resilient. Even in years that peak flows were substantially reduced and productivity was curtailed, prompt recoveries of NIRvP showed that cottonwoods were capable of rebuilding vigorous canopies and high photosynthetic activity with return of adequate root zone moisture. This owed to both mechanisms of avoidance and resistance preventing catastrophic xylem cavitation (Hultine et al., 2010; Tai et al., 2018; Tyree et al., 1994).

While the effects of river regulation on low flow characteristics were not apparent in the satellite record, the combined effects of reservoir trapping and offstream diversion on high flow characteristics were implicit in year-to-year patterns of NIRvP. Particularly in dry years, when irrigation demands were high, attenuated peak flows that limited root zone recharge had a direct negative impact on current-year productivity. Downstream reaches that were subject to the cumulative impacts of river regulation were the most impacted, notably the Lethbridge Reach owing to diversions and reservoirs along the heavily allocated southern tributaries (Figure 3.8). Downstream reaches that are further within the prairie region are also increasingly arid (Figure 3.9); presumably, this would enhance vulnerability to drought stress, however cottonwoods have likely adapted to local climate conditions. Prairie cottonwoods—a dry ecoregion species—also increase in abundance along these reaches. Whether systematic inter- and intra-specific variation in drought tolerance occurs to an extent that forests along some reaches are more predisposed to the impacts of river regulation

than others is an open question. Along the St. Mary River, narrowleaf cottonwoods and balsam poplars are found at the dry-limit of their range; the marginal suitability of conditions for their survival has been proposed as a predisposing factor to their half-century collapse from river regulation (Rood et al., 1995).

The Brocket Reach was not diverted, however it was subject to streamflow regulation from reservoir trapping in post-dam years. Depending on the balance between flow trapping and release, reservoir storage could have supplemented naturally occurring flows, or imposed a dewatering effect downstream. The impact of the latter on productivity was evident during initial reservoir filling in 1992 (Figures 3.10, 3.11). In 2002, moderate re-filling occurred following multi-year draw-down of reservoir water levels during the preceding drought, however abundant precipitation and associated streamflow generation from spring storms compensated, in terms of forest water supply. Although net storage changes were probably negligible in other years, streamflow seasonality was impacted. Mismatches between the timing of high flows and the primary period of leaf expansion during the early growing season would presumably have a negative impact on productivity (Figure 3.8). Although a free-flowing reach was not studied in post-dam years, flow–productivity relationships along the Brocket Reach were indifferent between pre- and post-dam periods. Thus, the impact of streamflow regulation on productivity was either negligible or masked by ample precipitation and root zone water storage.

4.4 Variation within reaches

Although there were no long-term trends in productivity at the reach-scale, there were local nuances within reaches (Figures 3.12, 3.13). Without assessing clusters of change pixels on a case basis, e.g. through classification of spectral-temporal characteristics, or ground truthing, underlying causes can only be speculated. To the extent that interpretation is useful, a noteworthy finding was an emergent association between

change pixels and channel braiding, migration and abandonment. Shifts in the active river channel presumably altered alluvial groundwater regimes, having consequences for cottonwood moisture availability and productivity. Specifically, permanent rises (declines) in the average water table position would have been favourable (stressful) for cottonwoods. Chronic water table declines associated with river channel migration perhaps pose analogues for severe river regulation and a natural experiment for studying cottonwood impacts. Larger patches of pixels with declining NIRvP, associated with avulsion events following the 1995 flood, have been noted upstream of the Brocket Reach. Although not tested, there were likely also variations in the moisture sensitivity of riparian forests (Mayes et al., 2020), owing to factors such as floodplain position (Rood et al., 2013; Tai et al., 2018), competition for resources between trees (Stromberg & Patten, 1996; Willms et al., 2006), levels of morbidity (Schook et al., 2020), trait variation across cottonwood genotypes, ages, and sexes, or the presence of novel water sources such as nearby irrigated cropland or leaky irrigation canals.

4.5 Implications for ecosystem health, dam operations and climate change

The resilience of riparian forests that was displayed in the satellite record is a defining characteristic of a healthy ecosystem (Rapport et al., 1998). However, there is a possible caveat to this claim. Assessing ecosystem resilience requires knowledge of ecological conditions both before and after the stress triggering event, yet the satellite record itself began during a period of unfavourable conditions (Figure 2.2). On one hand, it cannot be ruled out that riparian forests were more vigorous during the 1960's and early–mid 1970's, with productivity declining in subsequent years. On the other hand, growth declines and dieback of cottonwoods typically occur over decades (Rood et al., 1995; Schook et al., 2020). Tree ring records also support that cottonwoods downstream of the Waterton Dam have responded positively to

functional flows, now displaying naturalized growth patterns that mirror growth along upstream reaches (Foster et al., 2018). A similar chronology for the Oldman River would provide insightful historical context, as would extension of the satellite record by leveraging the first twelve years (1972–1983) of Multi Spectral Scanner imagery from the Landsat archive.

The survival of cottonwoods as a population fundamentally depends on rates of recruitment and mortality. The apparent resilience of riparian forests offers some insight into mortality, in that resilient individuals are less likely to succumb to stressful conditions. In contrast, individuals incapable of avoiding or resisting large losses of plant hydraulic conductance during drought conditions would presumably suffer from impaired future resource capture—hence productivity—and stress tolerance, thus survival (Anderegg et al., 2013; Hultine et al., 2010; Schook et al., 2020). It cannot be ruled out that some forest patches displaying declining NIRvP reflected cottonwoods that were less resistant to the negative impacts of river regulation. Do these long-term declines equate with losses of individuals or progressive growth declines that tend to precede mortality (Rogers et al., 2018; Schook et al., 2020)? Not necessarily, since partial dieback can provide a negative feedback mechanism during drought conditions by reducing water demand, restoring plant water relations, and permitting survival (Rood et al., 2000; Williams & Cooper, 2005). What is more certain is that total collapse of a foundation species is not a prerequisite for loss of ecological function and biodiversity (Ellison et al., 2005). Nonetheless, the small areal extent and spatial patchiness of these declines likely have negligible consequences for ecosystem health at the scale of the riparian corridor.

The apparent resilience of riparian forests suggests that some flexibility may be offered in terms of current water allocations. This includes loosened minimum flow requirements, possibly on a case basis depending on climatic and hydrological context and whether they permit the survival of more drought vulnerable seedlings and meet

the instream flow needs of aquatic organisms such as fish. A variety of tools may be useful for aiding water managers in decision making. This includes the use of real-time information on hydrology and tree- or ecosystem-scale physiological activity at extensively instrumented sites, and calibrated remote sensing proxies for spatial scaling and historical contextualization. These data streams would also provide forcing or constraint for prognostic models predicting plant responses to water supply under different dam operating scenarios. Plant hydraulics represents a particularly robust modelling framework, since it predicts the climatic and hydrological conditions leading to levels of hydraulic dysfunction that tend to predispose individuals to mortality (Sperry & Love, 2015; Tai et al., 2018). Ideally, dams would be operated to prevent downstream cottonwoods from exceeding such thresholds to their function.

Under current conditions, the outlook on the health of cottonwood forests along the Oldman River is positive, as long as dam operations continue to permit seedling establishment following periodic flooding (Rood et al., 1998; Rood & Mahoney, 2000). However, past-century streamflow records show progressive declines associated with increasing human water withdrawals and hydroclimatic change from global warming (St. Jacques et al., 2010). With no sign that these patterns will soon cease, both humans and riparian forests are expected to face declining water supply throughout the foreseeable future (Rood et al., 2008; Schindler & Donahue, 2006; St. Jacques et al., 2013). The productivity, health, and survival of cottonwood forests in future climates may depend on factors that can ameliorate the impact of climate change on water availability. This includes the plasticity of key traits related to drought tolerance (Hultine et al., 2020), the response of plant water and carbon balances to the continuous rise in atmospheric carbon dioxide (De Kauwe et al., 2021), and patterns of precipitation during the growing season, which are less certain for the prairie region (Barrow & Sauchyn, 2019). Human climate change adaptations that influence how water is managed and used, such as the widespread adoption of innovations that

increase water use efficiency in human systems, will also be important. Such "slowing down" of climate change assumes that the increasing pressure on water supply is progressive through time. While cottonwoods have likely adapted to past drought cycles that are revealed in climate and streamflow reconstructions (Axelson et al., 2009; Sauchyn & Skinner, 2001), if severe and prolonged drought is to occur in a near future, the compounded effect of human water withdrawals will pose a novel stress environment for cottonwoods. Active conservation measures such as direct seeding of restoration plantings that have been bred for drought resistant traits may be necessary to increase the resilience of riparian forests in worst-case future climate scenarios (Hultine et al., 2020).

4.6 Conclusions

The Oldman River Dam has been operated with a functional flow regime since its completion almost thirty years ago, yet the impact of dam operations on mature cottonwoods has not been previously documented. The Landsat archive provided a dense historical proxy record of riparian cottonwood forest productivity, spanning both pre- and post-dam years, which showed to be meaningful based on its strong correlation with ground measurements of ecosystem gas exchange and annual cottonwood growth. The correlation of year-to-year patterns of productivity with both streamflow and a climatic soil moisture index supported the view that cottonwoods along the Oldman River are faculative phreatophytes with roots growing in a range of soil layers (Flanagan et al., 2019; Rood et al., 2011). Consequently, cottonwoods were moisture sensitive, but would have been flexible in water source. Water storage in the unsaturated zone presumably contributed to the apparent lack of response of riparian forests to unfavourable low flow conditions during pre-dam years. The intermittent nature of severe dewatering and an adaptive tolerance of cottonwoods to drought likely also contributed. The current health status of the riparian corridor is positive

and an optimization of dam operations is supported, which would allow for some water savings. However, climate change and economic expansion are posing ongoing pressures on water supply for riparian forests. Whether future riparian forests will continue to thrive, function at a state of reduced vigour (Smith et al., 1991; Williams & Cooper, 2005), or die-back is uncertain and will depend on factors such as their natural adaptive capacity, water management, and the occurrence of megadroughts. Results from this study are likely applicable to riparian forests across the semi-arid North American prairies and associated issues of river management and conservation.

References

Amlin, N. A., & Rood, S. B. (2001). Inundation tolerances of riparian willows and cottonwoods. *Journal of the American Water Resources Association*, *37*(6), 1709–1720.

Anderegg, W. R., Plavcová, L., Anderegg, L. D., Hacke, U. G., Berry, J. A., & Field, C. B. (2013). Drought's legacy: multiyear hydraulic deterioration underlies widespread aspen forest die-off and portends increased future risk. *Global Change Biology*, *19*(4), 1188–1196.

Andersen, D. C. (2016). Flow regime effects on mature *Populus fremontii* (fremont cottonwood) productivity on two contrasting dryland river floodplains. *The Southwestern Naturalist*, *61*(1), 8–17.

Axelson, J. N., Sauchyn, D. J., & Barichivich, J. (2009). New reconstructions of streamflow variability in the South Saskatchewan River Basin from a network of tree ring chronologies, Alberta, Canada. *Water Resources Research*, *45*(9).

Badgley, G., Anderegg, L. D., Berry, J. A., & Field, C. B. (2019). Terrestrial gross primary production: Using $\mathrm{NIR_V}$ to scale from site to globe. *Global Change Biology*, *25*(11), 3731–3740.

Badgley, G., Field, C. B., & Berry, J. A. (2017). Canopy near-infrared reflectance and terrestrial photosynthesis. *Science Advances*, *3*(3), e1602244.

Baldocchi, D. D., Ryu, Y., Dechant, B., Eichelmann, E., Hemes, K., Ma, S., ... others (2020). Outgoing near infrared radiation from vegetation scales with canopy photosynthesis across a spectrum of function, structure, physiological capacity and weather. *Journal of Geophysical Research: Biogeosciences*, e2019JG005534.

Barrow, E. M., & Sauchyn, D. J. (2019). Uncertainty in climate projections and time of emergence of climate signals in the western Canadian Prairies. *International Journal of Climatology*, *39*(11), 4358–4371.

Benson, R. D., & Rood, S. B. (2018). Bringing twentieth-century water projects into the twenty-first century: The case for revisiting dam operations in Alberta. *Canadian Water Resources Journal/Revue Canadienne des Ressources Hydriques*, *43*(3), 335–346.

Bolton, D. K., Gray, J. M., Melaas, E. K., Moon, M., Eklundh, L., & Friedl, M. A. (2020). Continental-scale land surface phenology from harmonized Landsat 8 and Sentinel-2 imagery. *Remote Sensing of Environment*, *240*, 111685.

Braatne, J. H., Rood, S. B., & Heilman, P. E. (1996). Life history, ecology, and conservation of riparian cottonwoods in North America. In R. F. Stettler, H. D. Bradshaw Jr., P. E. Heilman, & T. M. Hinckley (Eds.), *Biology of Populus and its Implications for Management and Conservation* (pp. 57–85). Ottawa, ON, Canada: NRC Research Press.

Bradley, C. E., Reintjes, F., & Mahoney, J. M. (1991). *The biology and status of riparian poplars in southern Alberta.* Edmonton, AB, Canada: World Wildlife Fund Canada and Alberta Forestry, Lands and Wildlife.

Dechant, B., Ryu, Y., Badgley, G., Zeng, Y., Berry, J. A., Zhang, Y., ... others (2020). Canopy structure explains the relationship between photosynthesis and sun-induced chlorophyll fluorescence in crops. *Remote Sensing of Environment*, *241*, 111733.

De Kauwe, M. G., Medlyn, B. E., & Tissue, D. T. (2021). To what extent can rising [CO_2] ameliorate plant drought stress? *New Phytologist*, *231*(6), 2118-2124.

Doody, T. M., Benger, S. N., Pritchard, J. L., & Overton, I. C. (2014). Ecological response of *Eucalyptus camaldulensis* (river red gum) to extended drought and flooding along the River Murray, South Australia (1997–2011) and implications for environmental flow management. *Marine and Freshwater Research*, *65*(12), 1082–1093.

Ellison, A. M., Bank, M. S., Clinton, B. D., Colburn, E. A., Elliott, K., Ford, C. R., ... others (2005). Loss of foundation species: consequences for the structure and dynamics of forested ecosystems. *Frontiers in Ecology and the Environment*, *3*(9), 479–486.

Field, C. B. (1991). Ecological scaling of carbon gain to stress and resource availability. In H. A. Mooney, E. J. Pell, & W. E. Winner (Eds.), *Response of Plants to Multiple Stresses* (pp. 35–65). San Diego, CA, United States: Academic Press.

Flanagan, L. B., & Adkinson, A. C. (2011). Interacting controls on productivity in a northern Great Plains grassland and implications for response to ENSO events. *Global Change Biology*, *17*(11), 3293–3311.

Flanagan, L. B., Orchard, T. E., Logie, G. S., Coburn, C. A., & Rood, S. B. (2017). Water use in a riparian cottonwood ecosystem: Eddy covariance measurements and scaling along a river corridor. *Agricultural and Forest Meteorology*, *232*, 332–348.

Flanagan, L. B., Orchard, T. E., Tremel, T. N., & Rood, S. B. (2019). Using stable isotopes to quantify water sources for trees and shrubs in a riparian cottonwood ecosystem in flood and drought years. *Hydrological Processes*, *33*(24), 3070–3083.

Foster, S. G., Mahoney, J. M., & Rood, S. B. (2018). Functional flows: an environmental flow regime benefits riparian cottonwoods along the Waterton River, Alberta. *Restoration Ecology*, *26*(5), 921–932.

Gómez-Sapiens, M. M., Jarchow, C. J., Flessa, K. W., Shafroth, P. B., Glenn, E. P., & Nagler, P. L. (2020). Effect of an environmental flow on vegetation growth and health using ground and remote sensing metrics. *Hydrological Processes*, *34*(8), 1682–1696.

Hogg, E. H., Barr, A. G., & Black, T. A. (2013). A simple soil moisture index for representing multi-year drought impacts on aspen productivity in the western Canadian interior. *Agricultural and Forest Meteorology*, *178*, 173–182.

Holden, C. E., & Woodcock, C. E. (2016). An analysis of Landsat 7 and Landsat 8 underflight data and the implications for time series investigations. *Remote Sensing of Environment*, *185*, 16–36.

Horton, J., Kolb, T. E., & Hart, S. (2001). Responses of riparian trees to interannual variation in ground water depth in a semi-arid river basin. *Plant, Cell & Environment*, *24*(3), 293–304.

Hultine, K. R., Allan, G. J., Blasini, D., Bothwell, H. M., Cadmus, A., Cooper, H. F., ... others (2020). Adaptive capacity in the foundation tree species *Populus fremontii*: implications for resilience to climate change and non-native species invasion in the American Southwest. *Conservation Physiology*, *8*(1), coaa061.

Hultine, K. R., Bush, S. E., & Ehleringer, J. R. (2010). Ecophysiology of riparian cottonwood and willow before, during, and after two years of soil water removal. *Ecological Applications*, *20*(2), 347–361.

Huntington, J., McGwire, K., Morton, C., Snyder, K., Peterson, S., Erickson, T., ... Allen, R. (2016). Assessing the role of climate and resource management on groundwater dependent ecosystem changes in arid environments with the Landsat archive. *Remote Sensing of Environment*, *185*, 186–197.

Jönsson, P., Cai, Z., Melaas, E., Friedl, M. A., & Eklundh, L. (2018). A method for robust estimation of vegetation seasonality from Landsat and Sentinel-2 time series data. *Remote Sensing*, *10*(4), 635.

Kranjcec, J., Mahoney, J. M., & Rood, S. B. (1998). The responses of three riparian cottonwood species to water table decline. *Forest Ecology and Management*, *110*(1-3), 77–87.

Lytle, D. A., & Poff, N. L. (2004). Adaptation to natural flow regimes. *Trends in Ecology & Evolution*, *19*(2), 94–100.

Mayes, M., Caylor, K. K., Singer, M. B., Stella, J. C., Roberts, D., & Nagler, P. (2020). Climate sensitivity of water use by riparian woodlands at landscape scales. *Hydrological Processes*, *34*(25), 4884–4903.

McNeeley, S. M., Friedman, J. M., Beeton, T. A., & Thaxton, R. D. (2020). *Cottonwoods, water, and people—integrating analysis of tree rings with observations of*

elders from the Eastern Shoshone and Northern Arapaho Tribes of the Wind River Reservation, Wyoming (Tech. Rep.).

Monteith, J. L., & Unsworth, M. H. (2013). *Principles of Environmental Physics: Plants, Animals, and the Atmosphere*. Academic Press.

Nagler, P. L., Barreto-Muñoz, A., Chavoshi Borujeni, S., Jarchow, C. J., Gómez-Sapiens, M. M., Nouri, H., ... Didan, K. (2020). Ecohydrological responses to surface flow across borders: Two decades of changes in vegetation greenness and water use in the riparian corridor of the Colorado River delta. *Hydrological Processes*, *34*(25), 4851–4883.

Nagler, P. L., Glenn, E. P., & Hinojosa-Huerta, O. (2009). Synthesis of ground and remote sensing data for monitoring ecosystem functions in the Colorado River Delta, Mexico. *Remote Sensing of Environment*, *113*(7), 1473–1485.

Nagler, P. L., Scott, R. L., Westenburg, C., Cleverly, J. R., Glenn, E. P., & Huete, A. R. (2005). Evapotranspiration on western US rivers estimated using the Enhanced Vegetation Index from MODIS and data from eddy covariance and Bowen ratio flux towers. *Remote Sensing of Environment*, *97*(3), 337–351.

Naiman, R. J., & Decamps, H. (1997). The ecology of interfaces: riparian zones. *Annual Review of Ecology and Systematics*, *28*(1), 621–658.

Naiman, R. J., Decamps, H., & Pollock, M. (1993). The role of riparian corridors in maintaining regional biodiversity. *Ecological Applications*, *3*(2), 209–212.

Nguyen, U., Glenn, E. P., Nagler, P. L., & Scott, R. L. (2015). Long-term decrease in satellite vegetation indices in response to environmental variables in an iconic desert riparian ecosystem: the Upper San Pedro, Arizona, United States. *Ecohydrology*, *8*(4), 610–625.

Oldman Waterhsed Council. (2010). *Oldman River State of the Watershed Report 2010.* Retrieved 2021-04-15, from `http://oldmanbasin.org/teams-andprojects/state-of-the-watershed-report/`

Patten, D. T. (1998). Riparian ecosytems of semi-arid North America: diversity and human impacts. *Wetlands*, *18*(4), 498–512.

Pekel, J.-F., Cottam, A., Gorelick, N., & Belward, A. S. (2016). High-resolution mapping of global surface water and its long-term changes. *Nature*, *540*(7633), 418–422.

Philipsen, L. J., Pearce, D. W., & Rood, S. B. (2018). Hydroclimatic drivers of the growth of riparian cottonwoods at the prairie margin: River flows, river regulation and the Pacific Decadal Oscillation. *Dendrochronologia*, *51*, 82–91.

Rapport, D. J., Costanza, R., & McMichael, A. (1998). Assessing ecosystem health. *Trends in Ecology & Evolution*, *13*(10), 397–402.

Rogers, B. M., Solvik, K., Hogg, E. H., Ju, J., Masek, J. G., Michaelian, M., ... Goetz, S. J. (2018). Detecting early warning signals of tree mortality in boreal North America using multiscale satellite data. *Global Change Biology*, *24*(6), 2284–2304.

Rood, S. B., Ball, D. J., Gill, K. M., Kaluthota, S., Letts, M. G., & Pearce, D. W. (2013). Hydrologic linkages between a climate oscillation, river flows, growth, and wood Δ^{13}C of male and female cottonwood trees. *Plant, Cell & Environment*, *36*(5), 984–993.

Rood, S. B., Bigelow, S. G., & Hall, A. A. (2011). Root architecture of riparian trees: River cut-banks provide natural hydraulic excavation, revealing that cottonwoods are facultative phreatophytes. *Trees*, *25*(5), 907.

Rood, S. B., Braatne, J. H., & Hughes, F. M. (2003). Ecophysiology of riparian cottonwoods: stream flow dependency, water relations and restoration. *Tree Physiology*, *23*(16), 1113–1124.

Rood, S. B., Kalischuk, A. R., & Mahoney, J. M. (1998). Initial cottonwood seedling recruitment following the flood of the century of the Oldman River, Alberta, Canada. *Wetlands*, *18*(4), 557–570.

Rood, S. B., & Mahoney, J. M. (2000). Revised instream flow regulation enables cottonwood recruitment along the St. Mary River, Alberta, Canada. *Rivers*, *7*(2), 109–125.

Rood, S. B., Mahoney, J. M., Reid, D. E., & Zilm, L. (1995). Instream flows and the decline of riparian cottonwoods along the St. Mary River, Alberta. *Canadian Journal of Botany*, *73*(8), 1250–1260.

Rood, S. B., Pan, J., Gill, K. M., Franks, C. G., Samuelson, G. M., & Shepherd, A. (2008). Declining summer flows of Rocky Mountain rivers: Changing seasonal hydrology and probable impacts on floodplain forests. *Journal of Hydrology*, *349*(3-4), 397–410.

Rood, S. B., Patiño, S., Coombs, K., & Tyree, M. T. (2000). Branch sacrifice: cavitation-associated drought adaptation of riparian cottonwoods. *Trees*, *14*(5), 248–257.

Rood, S. B., Samuelson, G. M., Braatne, J. H., Gourley, C. R., Hughes, F. M., & Mahoney, J. M. (2005). Managing river flows to restore floodplain forests. *Frontiers in Ecology and the Environment*, *3*(4), 193–201.

Rood, S. B., & Vandersteen, J. W. (2010). Relaxing the principle of prior appropriation: Stored water and sharing the shortage in Alberta, Canada. *Water Resources Management*, *24*(8), 1605–1620.

Roy, D. P., Kovalskyy, V., Zhang, H., Vermote, E. F., Yan, L., Kumar, S., & Egorov, A. (2016). Characterization of Landsat-7 to Landsat-8 reflective wavelength and

normalized difference vegetation index continuity. *Remote Sensing of Environment*, *185*, 57–70.

Roy, D. P., Zhang, H., Ju, J., Gomez-Dans, J. L., Lewis, P. E., Schaaf, C., ... Kovalskyy, V. (2016). A general method to normalize Landsat reflectance data to nadir BRDF adjusted reflectance. *Remote Sensing of Environment*, *176*, 255–271.

Sauchyn, D. J., & Skinner, W. R. (2001). A proxy record of drought severity for the southwestern Canadian Plains. *Canadian Water Resources Journal*, *26*(2), 253–272.

Schindler, D. W., & Donahue, W. F. (2006). An impending water crisis in Canada's western prairie provinces. *Proceedings of the National Academy of Sciences*, *103*(19), 7210–7216.

Schook, D. M., Friedman, J. M., Stricker, C. A., Csank, A. Z., & Cooper, D. J. (2020). Short-and long-term responses of riparian cottonwoods (*Populus spp.*) to flow diversion: Analysis of tree-ring radial growth and stable carbon isotopes. *Science of the Total Environment*, *735*, 139523.

Sellers, P. J. (1987). Canopy reflectance, photosynthesis, and transpiration, II. the role of biophysics in the linearity of their interdependence. *Remote Sensing of Environment*, *21*(2), 143–183.

Smith, S. D., Wellington, A. B., Nachlinger, J. L., & Fox, C. A. (1991). Functional responses of riparian vegetation to streamflow diversion in the eastern Sierra Nevada. *Ecological Applications*, *1*(1), 89–97.

Sperry, J. S., & Love, D. M. (2015). What plant hydraulics can tell us about responses to climate-change droughts. *New Phytologist*, *207*(1), 14–27.

St. Jacques, J.-M., Lapp, S. L., Zhao, Y., Barrow, E. M., & Sauchyn, D. J. (2013). Twenty-first century central Rocky Mountain river discharge scenarios under greenhouse forcing. *Quaternary International*, *310*, 34–46.

St. Jacques, J.-M., Sauchyn, D. J., & Zhao, Y. (2010). Northern Rocky Mountain streamflow records: Global warming trends, human impacts or natural variability? *Geophysical Research Letters*, *37*(6).

Stromberg, J. C. (2001). Restoration of riparian vegetation in the south-western United States: importance of flow regimes and fluvial dynamism. *Journal of Arid Environments*, *49*(1), 17–34.

Stromberg, J. C., & Patten, D. T. (1990). Riparian vegetation instream flow requirements: a case study from a diverted stream in the eastern Sierra Nevada, California, USA. *Environmental Management*, *14*(2), 185–194.

Stromberg, J. C., & Patten, D. T. (1996). Instream flow and cottonwood growth in the eastern Sierra Nevada of California, USA. *Regulated Rivers: Research & Management*, *12*(1), 1–12.

Sulla-Menashe, D., Friedl, M. A., & Woodcock, C. E. (2016). Sources of bias and variability in long-term Landsat time series over Canadian boreal forests. *Remote Sensing of Environment*, *177*, 206–219.

Tai, X., Mackay, D. S., Sperry, J. S., Brooks, P., Anderegg, W. R., Flanagan, L. B., ... Hopkinson, C. (2018). Distributed plant hydraulic and hydrological modeling to understand the susceptibility of riparian woodland trees to drought-induced mortality. *Water Resources Research*, *54*(7), 4901–4915.

Thornton, P. E., Running, S. W., & White, M. A. (1997). Generating surfaces of daily meteorological variables over large regions of complex terrain. *Journal of Hydrology*, *190*(3-4), 214–251.

Tyree, M. T., Kolb, K. J., Rood, S. B., & Patiño, S. (1994). Vulnerability to drought-induced cavitation of riparian cottonwoods in Alberta: a possible factor in the decline of the ecosystem? *Tree Physiology*, *14*(5), 455–466.

Williams, C. A., & Cooper, D. J. (2005). Mechanisms of riparian cottonwood decline along regulated rivers. *Ecosystems*, *8*(4), 382–395.

Willms, C. R., Pearce, D. W., & Rood, S. B. (2006). Growth of riparian cottonwoods: a developmental pattern and the influence of geomorphic context. *Trees*, *20*(2), 210–218.

Wu, G., Guan, K., Jiang, C., Peng, B., Kimm, H., Chen, M., ... others (2020). Radiance-based NIR_v as a proxy for GPP of corn and soybean. *Environmental Research Letters*, *15*(3), 034009.

Yang, H., Rood, S. B., & Flanagan, L. B. (2019). Controls on ecosystem water-use and water-use efficiency: Insights from a comparison between grassland and riparian forest in the northern Great Plains. *Agricultural and Forest Meteorology*, *271*, 22–32.

Yue, S., Pilon, P., Phinney, B., & Cavadias, G. (2002). The influence of autocorrelation on the ability to detect trend in hydrological series. *Hydrological Processes*, *16*(9), 1807–1829.

Zeng, Y., Badgley, G., Dechant, B., Ryu, Y., Chen, M., & Berry, J. A. (2019). A practical approach for estimating the escape ratio of near-infrared solar-induced chlorophyll fluorescence. *Remote Sensing of Environment*, *232*, 111209.

Zhao, Y., Wei, Y., Li, S., & Wu, B. (2016). Downstream ecosystem responses to middle reach regulation of river discharge in the Heihe River Basin, China. *Hydrology and Earth System Sciences*, *20*(11), 4469–4481.

Appendix A

Harmonizing Landsat Surface Reflectance

Methods

To normalize surface reflectance to a common sensor, the method of Roy, Kovalskyy, et al. (2016) was adopted, which leverages image overlap with one-day separation between Landsat 5 and 7, and Landsat 7 and 8 across adjacent (east–west) World Reference System-2 (WRS-2) Paths. Consequently, the Landsat 5 Thematic Mapper (TM) and Landsat 8 Operational Land Imager (OLI) were normalized to the Landsat 7 Enhanced Thematic Mapper Plus (ETM+). A collection of TM/ETM+ (n = 10) and ETM+/OLI (n = 8) image pairs were curated. For each pair on a band basis, pixels were randomly sampled from five evenly spaced reflectance classes and combined across pairs. An evenly sized sample from the east and west image margins was ensured so that view angle effects canceled-out (Roy, Kovalskyy, et al., 2016). Lastly, the accumulated pixel samples were regressed using ordinary linear regression to generate gains and offsets that predicted ETM+-like reflectance. To account for view angle effects on surface reflectance across WRS-2 Paths (Sulla-Menashe et al., 2016), the same sample pixels were then grouped by WRS-2 Path and regressions were repeated to predict reflectance as if viewed from the central WRS-2 Path (Path 41). This two-step procedure was repeated for 500 random samples and the median linear models were reported, with 95% confidence intervals constructed from the 2.5 and 97.5 percentiles. A second regression that was forced through the origin was also tested.

To assess the radiometric continuity of the Landsat archive for historical ecosystem health assessments using the near-infrared reflectance of vegetation (NIRv), NIRv derived from harmonized and un-harmonized TM/ETM+/OLI and Moderate Resolution Imaging Spectroradiometer (MODIS) surface reflectance were compared. NIRv was not adjusted for variation in dormant season reflectance here. MODIS NIRv was derived from the MCD43A4 version 6 product, which predicts daily nadir-adjusted surface reflectance by combining observations within a 16-day window. The product was available for the entire MODIS era (2000–present) at a 500 m resolution and was accessed via the Google Earth Engine. Since MODIS was expected to be radiometrically stable, it represented a standard reference for harmonizing TM/ETM+/OLI. Comparisons of NIRv were made over a homogeneous grazed grass surface, contained in the footprint of a single MODIS pixel, within the Animal Disease Research Insti-

tute in Lethbridge, Alberta, Canada. First, ETM+ and MODIS NIRv were regressed to predict MODIS. Then, the regression line was used to predict MODIS from TM and OLI. If TM and OLI were successfully normalized to ETM+, the prediction error would presumably be small. Agreement was quantified using the bias and root mean squared error (RMSE)

$$\text{Bias} = \frac{1}{N}\sum_{i=1}^{N}\left(\hat{\rho}_i^{MODIS} - \rho_i^{MODIS}\right) \tag{A.1}$$

$$\text{RMSE} = \sqrt{\frac{1}{N}\sum_{i=1}^{N}\left(\hat{\rho}_i^{MODIS} - \rho_i^{MODIS}\right)^2} \tag{A.2}$$

where ρ^{MODIS} is the actual MODIS reflectance and $\hat{\rho}^{MODIS}$ is the predicted MODIS reflectance from TM or OLI. Bias and RMSE were normalized by dividing by $\overline{\hat{\rho}^{MODIS}}$.

Results

Gains and offsets to normalize TM and OLI surface reflectance to ETM+ are listed in Table A.1 and examples of scatterplots of reflectance between sensors are shown in Figures A.1 and A.2. Gains and offsets to normalize surface reflectance from WRS-2 Paths 40 and 42 to values as if viewed from Path 41 are listed in Table A.2 and examples of scatterplots of reflectance between WRS-2 Paths are shown in Figures A.3 and A.4.

Based on the evaluation using MODIS, NIRv was estimated to be 1.9% darker for TM than ETM+ and 8.4% brighter for OLI than ETM+ (Table A.3). The two parameter model (gain and offset) was unsuccessful at reducing the TM–ETM+ bias, but reduced the the OLI–ETM+ bias to within 1%. The single parameter model (only gain) reduced the TM–ETM+ and OLI–ETM+ biases to within 1% and 2.5%, respectively. The width of 95% confidence intervals ranged from 3–6%, indicating that the success of sensor normalization depended on image sampling to some extent. The harmonized data products slightly reduced the RMSE between predicted and actual MODIS NIRv (Table A.4).

Discussion

Discrepancies in surface reflectance among sensors did not entirely align with what has been reported in the literature on a band basis. For example, while OLI has been reported to be darker and slightly brighter than ETM+ for visible and infrared bands, respectively (Holden & Woodcock, 2016), only the latter was supported. However, inter-sensor biases in NIRv agreed with previously reported biases in the normalized difference vegetation index (Holden & Woodcock, 2016; Sulla-Menashe et al., 2016; Roy, Kovalskyy, et al., 2016). Thus, it seemed that relative biases among sensors were somewhat preserved—at least for the red and near-infrared bands.

At the overlapping image margin between adjacent WRS-2 Paths, lower (higher) reflectance in Path 41 images than Path 40 (42) images agreed with the typical effect

Table A.1: Slopes and offsets from ordinary least squares (OLS) regression to normalize TM and OLI surface reflectance to ETM+. Model coefficients are medians [95% confidence intervals] from 500 random samples.

Band	Sensor	OLS		OLS (no offset)
		Gain	Offset	Slope
B	TM	0.905 [0.855, 0.921]	0.003 [0.002, 0.007]	0.941 [0.928, 0.948]
B	OLI	0.873 [0.842, 0.905]	0.009 [0.007, 0.011]	0.992 [0.976, 1.007]
G	TM	0.903 [0.806, 0.916]	0.002 [0.001, 0.011]	0.919 [0.896, 0.925]
G	OLI	0.877 [0.847, 0.898]	0.005 [0.004, 0.008]	0.926 [0.916, 0.936]
R	TM	1.000 [0.931, 1.011]	−0.003 [−0.005, 0.004]	0.976 [0.957, 0.982]
R	OLI	0.896 [0.874, 0.916]	0.010 [0.008, 0.012]	0.976 [0.965, 0.986]
NIR	TM	0.971 [0.960, 0.981]	0.009 [0.005, 0.012]	0.995 [0.990, 1.000]
NIR	OLI	0.951 [0.938, 0.963]	0.004 [−0.001, 0.008]	0.959 [0.952, 0.965]
SWIR1	TM	0.972 [0.962, 0.982]	0.003 [0.001, 0.005]	0.983 [0.978, 0.988]
SWIR1	OLI	0.961 [0.944, 0.976]	0.010 [0.006, 0.013]	1.000 [0.992, 1.007]
SWIR2	TM	0.958 [0.946, 0.970]	0.006 [0.004, 0.009]	0.987 [0.981, 0.993]
SWIR2	OLI	0.960 [0.941, 0.979]	0.005 [0.002, 0.008]	0.985 [0.977, 0.994]

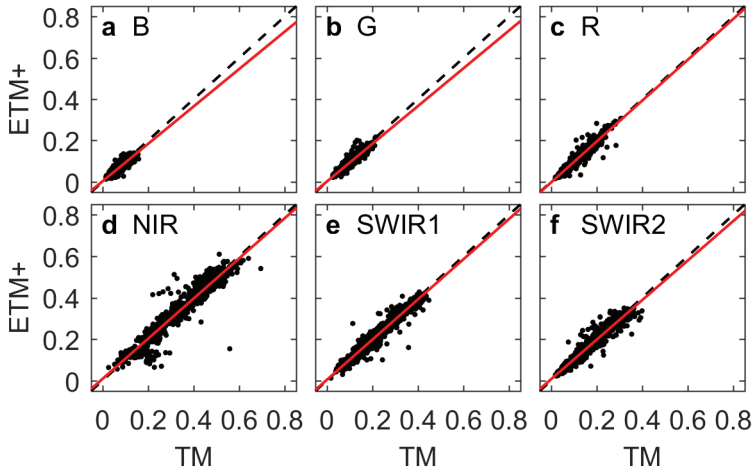

Figure A.1: Scatterplots of TM and ETM+ surface reflectance for six common reflective wavebands. Solid lines are ordinary regression lines and dashed lines are 1:1

.

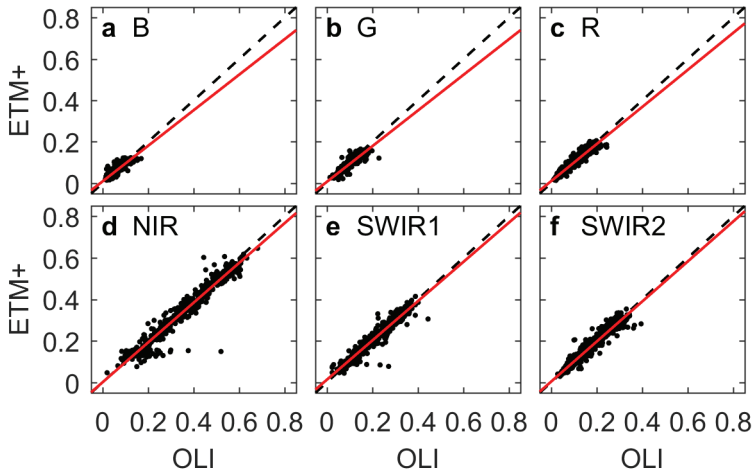

Figure A.2: Same as Figure A.1 but comparing OLI and ETM+.

Table A.2: Slopes and offsets from ordinary least squares (OLS) regression to normalize surface reflectance from overlapping World Reference System-2 (WRS-2) Paths 40 and 42 to Path 41. Model coefficients are medians [95% confidence intervals] from 500 random samples.

Band	WRS-2 Path	OLS		OLS (no offset)
		Gain	Offset	Slope
B	40	0.985 [0.968, 1.015]	−0.006 [−0.008, −0.005]	0.906 [0.900, 0.913]
B	42	1.153 [1.093, 1.181]	−0.001 [−0.003, 0.002]	1.143 [1.129, 1.156]
G	40	0.984 [0.972, 1.043]	−0.006 [−0.010, −0.005]	0.932 [0.927, 0.945]
G	42	1.092 [1.006, 1.110]	−0.000 [−0.001, 0.006]	1.094 [1.068, 1.101]
R	40	0.963 [0.952, 0.999]	−0.004 [−0.008, −0.003]	0.929 [0.924, 0.939]
R	42	1.070 [1.024, 1.084]	0.002 [0.001, 0.006]	1.086 [1.068, 1.094]
NIR	40	0.994 [0.985, 1.002]	−0.012 [−0.015, −0.009]	0.961 [0.958, 0.965]
NIR	42	1.040 [1.030, 1.050]	0.004 [0.001, 0.006]	1.052 [1.047, 1.056]
SWIR1	40	0.985 [0.976, 0.994]	−0.010 [−0.012, −0.008]	0.946 [0.942, 0.951]
SWIR1	42	1.056 [1.047, 1.066]	0.002 [0.001, 0.004]	1.067 [1.062, 1.073]
SWIR2	40	0.980 [0.969, 0.990]	−0.008 [−0.010, −0.007]	0.940 [0.936, 0.945]
SWIR2	42	1.080 [1.066, 1.092]	−0.000 [−0.002, 0.002]	1.081 [1.074, 1.087]

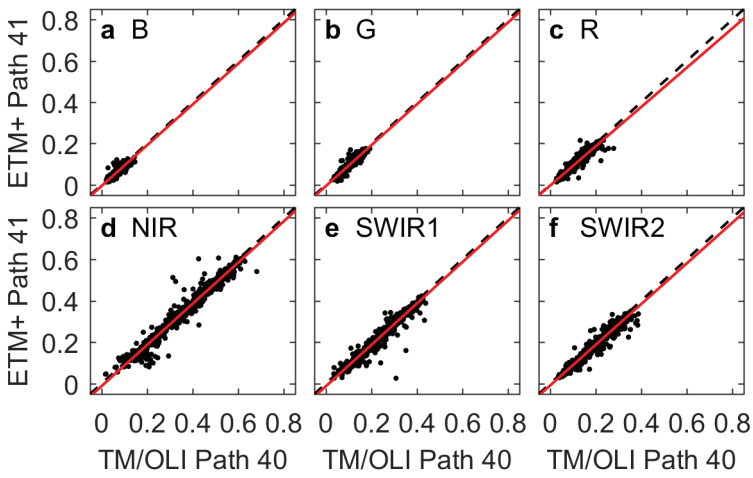

Figure A.3: Scatterplots of harmonized TM, ETM+, and OLI surface reflectance between overlapping World Reference System-2 (WRS-2) Paths 40 and 41 for for six common reflective wavebands. Solid lines are ordinary regression lines and dashed lines are 1:1

.

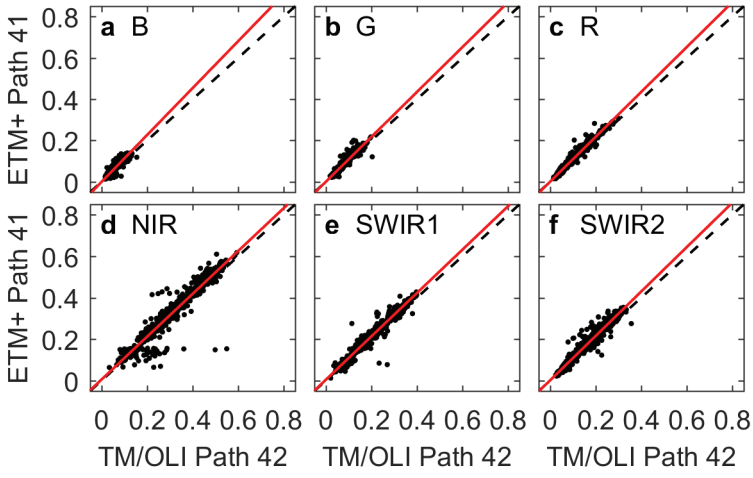

Figure A.4: Same as Figure A.3 but comparing WRS-2 Paths 42 and 41.

Table A.3: Estimated biases between TM or OLI and ETM+ derived NIRv before and after harmonization, based on evaluation against MODIS. Biases are medians [95% confidence intervals] from 500 model realizations.

Sensor	Bias (%)		
	Un-harmonized	Harmonized OLS	Harmonized OLS (no offset)
TM	−1.89	2.34 [0.20, 4.44]	0.43 [−0.86, 2.09]
OLI	8.41	−0.85 [−4.41, 2.45]	2.53 [0.67, 4.49]

Table A.4: Same as Table A.3 but for root mean squared errors (RMSE).

Sensor	RMSE (%)		
	Un-harmonized	Harmonized OLS	Harmonized OLS (no offset)
TM	9.17	8.65 [8.46, 9.16]	9.04 [8.91 9.31]
OLI	12.03	10.70 [10.21, 12.03]	9.51 [9.43, 9.82]

of Landsat's viewing geometry on reflectance retrievals (Roy, Zhang, et al., 2016). Specifically, Landsat's viewing geometry is such that where reflectance is retrieved in forward scattering mode along one WRS-2 Path, it is retrieved in backward scattering mode along the other (Roy, Zhang, et al., 2016). Reflectance retrievals are typically brighter in the former viewing configuration than the latter. Underlying mechanisms for this includes shadow casting, which results in different sunlit versus shade fractions between configurations (Roy, Zhang, et al., 2016; Sulla-Menashe et al., 2016). Thus, while leveraging images from overlapping WRS-2 Paths was desirable in terms of enhancing image availability, view angle effects on reflectance may have introduced a source of error and bias if had not been addressed.

Inter-sensor biases could have caused a spurious positive trend in NIRv if not accounted for. The harmonized data product was not perfect, based on evaluation against MODIS, yet the magnitude of inter-sensor biases was reduced. Normalization equations for regional or general applications can be found in the existing literature, however the magnitude of biases have been noted to vary temporally and spatially due to factors such as landcover and atmosphere (Holden & Woodcock, 2016). To explore this, popularly used equations from Roy, Kovalskyy, et al. (2016) (Table 2, ordinary least squares regressions) were tested. Based on the same evaluation against MODIS, these equations failed to reduce the bias in NIRv. Thus, developing a harmonized data product from local observations was worthwhile.

The two parameter model was more flexible than the single parameter model, however parameters for the former generally had higher error margins than parameters for the latter. The dependency of biases on image sampling may have been due to unmasked cloud, cloud shadow, and haze. Alternatively, sampled land cover may have been important. The harmonized data product can likely be improved by more strategic image sampling. For the rest of the study, the single parameter model was selected, which seemed to be the slightly more consistent model.

Appendix B

Supporting Information

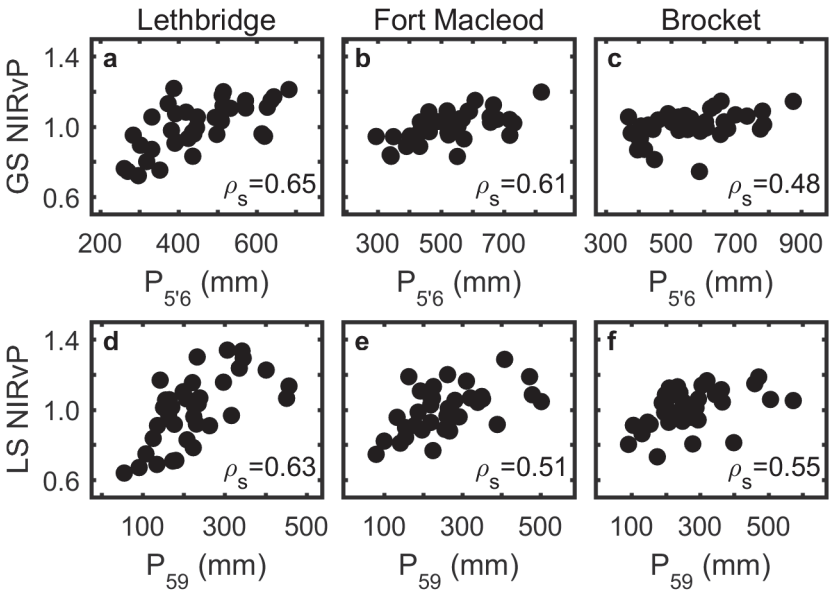

Figure B.1: Relationships between (a,b,c) the growing season integrated (GS) NIRvP and prior May–current June precipitation ($P_{5'6}$), and (d,e,f) the late summer (LS) NIRvP and May–September precipitation (P_{56}) along the (a,d) Lethbridge, (b,e) Fort Macleod, and (c,f) Brocket Reaches. Spearman's rank correlation coefficients (ρ_s) are noted.